Article

Low-Cost Open-Source Melt Flow Index System for Distributed Recycling and Additive Manufacturing

Dawei Liu , Aditi Basdeo , Catalina Suescun Gonzalez , Alessia Romani , Hakim Boudaoud , Cécile Nouvel , Fabio A. Cruz Sanchez , Joshua M. Pearce *

Posted Date: 29 September 2024

doi: 10.20944/preprints202409.2305.v1

Keywords: material extrusion; material properties; melt flow index; open hardware; polymers; recycling; rheology; thermal properties

Article

Low-Cost Open-Source Melt Flow Index System for Distributed Recycling and Additive Manufacturing

Dawei Liu [1], Aditi Basdeo [2,3], Catalina Suescun Gonzalez [4,5], Alessia Romani [1], Hakim Boudaoud [4], Cécile Nouvel [5], Fabio A. Cruz Sanchez [4] and Joshua M. Pearce [1,3,*]

[1] Department of Electrical and Computer Engineering, Western University, London, Canada
[2] Department of Chemical and Biochemical Engineering, Western University, London, Canada
[3] Ivey Business School, Western University, London, Canada
[4] Université de Lorraine, ERPI, F-54000, Nancy, France
[5] Université de Lorraine, CNRS, LRGP, F-54000 Nancy, France
* Correspondence: joshua.pearce@uwo.ca

Abstract: The increasing adoption of distributed recycling via additive manufacturing (DRAM) has facilitated the revalorization of materials derived from waste streams for additive manufacturing. Recycled materials frequently contain impurities and mixed polymers, which can degrade their properties over multiple cycles. This degradation, particularly in rheological properties, limits their applicability in 3D printing. Consequently, there is a critical need for a tool that enables rapid assessment of the flowability of these recycled materials. This study presents the design, development, and manufacturing of an open-source melt flow index (MFI) apparatus. The proposed MFI tool offers a user-friendly and cost-effective solution for evaluating the flow properties of materials from waste streams, thereby enhancing their viability for additive manufacturing applications.

Keywords: material extrusion; material properties; melt flow index; open hardware; polymers; recycling; rheology; thermal properties

1. Introduction

Due to a wide range of beneficial properties, synthetic polymers generally derived from fossil fuels are in widespread use, as over 390 million metric tons of plastic are produced globally [1]. One property, which has turned out to be something of a curse, is that most plastics have great durability and are resistant to degradation, enabling them to persist as environmental pollutants for hundreds of years [2]. When not properly disposed, plastics can cause environmental pollution [3], harming wildlife and ecosystems, [4] as well as humans [5,6]. Therefore, it is important to manage the waste plastic and recycle it to minimize the harm caused by wasted plastic to benefit both the environment and humanity [7]. Unfortunately, only 9% of plastic has been recycled [8]. Of the rest, half is landfilled, 22% is mismanaged, and 19% is burned or incinerated [8]. Of the unrecycled plastics, thermoplastics present a substantial opportunity to profitably utilize available materials, reduce pollution, and redirect waste from landfills. A new approach to developing a circular economy for plastics is being developed in the additive manufacturing industry (AM). It has been shown to be profitable [9,10] using the process of distributed recycling for additive manufacturing (DRAM) [11,12]. In this model, prosumers (a portmanteau of producing consumers) have a direct economic benefit by offsetting purchase of plastic products by recycling their waste into custom open-source products [10]. This model is in contrast to traditional centralized recycling models for plastic, which provide no incentive to consumers because of the low value of low density of collecting and transporting post-consumer plastic waste [12]. DRAM plastic converted to AM feedstock will increase in value between 4x and 20x as the value of bulk commercial plastic pellets ($1-5/kg) or commercial filament (~$20/kg). With DRAM, greenhouse gas (GHG) emissions from the embodied

 doi:10.20944/preprints202409.2305.v1

energy of transportation are minimized for AM materials [13,14]. This result is possible in the most extreme case of consumers manufacturing their own products from their own waste in their own homes [15,16]. Further reductions in GHG emissions are possible when DRAM uses renewable energy like solar photovoltaic technology [17,18]. Community-level DRAM using a recycling network is also feasible [19,20] and still more efficient than centralized recycling [21]. Overall, DRAM models challenge global value chains already under assault with distributed manufacturing [22].

In order to facilitate DRAM, open source (OS) waste plastic extruders called recyclebots [23], [24] have been developed to provide filament feedstock for Fused Filament Fabrication (FFF) processes. Recycled waste plastic filaments can be used in any low-cost self-replicating rapid prototype (RepRap)-class [25–27] 3D printer. A wide range of recycled plastic has already been shown to be DRAM compatible:

- polylactic acid (PLA) [28–30],
- acrylonitrile butadiene styrene (ABS) [10,31],
- high-density polyethylene (HDPE) [23,32,33],
- poly(ethylene terephthalate) (PET) [34,35],
- linear low-density polyethylene (LLDPE) and low-density polyethylene (LDPE) [36,37],
- polypropylene (PP) and polystyrene (PS) [33],
- elastomers [38],
- carbon-reinforced plastic composites [39],
- waste wood fiber reinforced plastics [35,40]
- fiber-filled composites [41,42].

Furthermore, the filament-making step can be avoided by 3D printing directly from shredded waste in Fused Particle Fabrication (FPF) / Fused Granular Fabrication (FGF) systems [43,44]. Using direct screw-assisted extruders, either single- or twin-screw systems, further expands the range of available DRAM materials [1,45], including polymer blends and multi-material recycling thermoplastics [46,47], multiple-recycled flake feedstocks [43,48], and bio-based thermoplastics or composites [49–51]. Moreover, it improves the economics of DRAM [47,51,52], reducing the cost of producing the material and environmental pollution [54].

There are, however, challenges remaining in DRAM, especially focusing on the materials qualification step. For example, different types of polymers require distinct recycling processes, making proper sorting essential [55]. Impurities, contaminants, and the complexities of recycling multi-polymer waste streams pose significant challenges due to incompatibility issues. These impurities affect overall processability, such as flowability and printability, and diminish technical properties, e.g., mechanical and rheological properties. At the same time, incompatibilities increase material heterogeneity, making it difficult to accurately predict changes in properties. For unknown plastics of different types, rapid characterization methods can help to identify the potential processability of the material to be used in DRAM, reducing the impacts and scraps generated in the initial tuning of the 3D printing setup. One proposed method is the melt flow index (MFI) measurement, which is a good reference for the melt flow behavior of a thermoplastic material, hence its flowability during the 3D printing process [56,57]. MFI, or melt flow rate (MFR), measures the ability of the molten polymer mass to flow through an orifice or die below a heated barrel under a given loading pressure and temperature for a given amount of time [58], usually measured in g/10min. MFI is a proxy index feature related to the material's molecular weight [59], which means it can provide information about the material's viscosity and flowability, allowing a better understanding of its potential behavior in the 3D printer [55]. It should be noted that MFI is measured at a low shear rate compared to the real stress during 3D printing. In general, the higher is the MFI, the lower are the viscosity and molecular weight of the tested material, increasing the flow per unit time. This value can be used to determine other properties, e.g., melt volume rate (MVR) and intrinsic viscosity, giving further insight into the rheological behavior of the material [60]. MFI also helps set an initial melt temperature without the need for more complex characterization methods, such as differential scanning calorimetry (DSC). Although other thermal properties also affect printability in FFF/FGF, e.g., crystallinity index [61], the immediacy of MFI measurements and the availability of

 doi:10.20944/preprints202409.2305.v1

standardized methods make it an accessible and reliable way to assess the printability of thermoplastics [62]. For DRAM operationalized at the community scale, MFI represents a potential means to quickly screen potential AM feedstock materials [56,63], as the material characteristics could be changed after one or multiple recycling processes due to thermomechanical degradation of thermoplastics during the recycling and extrusion steps [43,64]. For example, the MFI of ABS will increase after recycling due to degradation, leading to a decrease in its viscosity [65], and hence, its flowability increases. Thus, new 3D printing temperatures or speeds may be applied. In addition, MFI is not only used to assess the behavior of pure thermoplastic materials; it also provides a quick evaluation of the flowability and printability of materials that contain additives, such as compatibilizers [66], chain extenders [67,68], fillers [69], and bio-sourced components [70,71], further expanding its use.

To rapidly assess the printability of recycled materials, MFI presents a viable and rapid alternative to complex and longer rheological measurements [72,73]. Unfortunately, proprietary MFI systems are still expensive, ~CAD$4,700 from Amazon [74] and ~CAD$2,000 from AliExpress [75]. This fact limits accessibility to resource-constrained settings for which DRAM is perhaps the most promising because prosumers could trade their labor for high-value products for themselves or to sell. Furthermore, exploiting rapid characterization tools for DRAM could improve the overall quality of the 3D printed products produced by the prosumers, hence increasing the adoption of this technology and its reliability for product applications, e.g., reducing failures and material scraps from parameter tuning.

To address this issue, this article introduces a low-cost open-source Melt Flow Index er. First, the basic functioning of an MFI is outlined. The operation and design of each of the major subassemblies of the OS MFI device are then detailed. The complete bill of materials (BOM) and assembly instructions are provided in Appendix A and B. Next, the OS MFI device is validated against a gold-standard commercial MFI and then used for the MFI assessment of some common thermoplastics, including waste plastics for DRAM: virgin PLA pellets, shredded recycled poly(ethylene) terephthalate glycol (PETG) flakes, and recycled HDPE/ PET flake blends. The results are compared and discussed in the context of DRAM.

2. Materials and Methods

An MFI device is a measuring tool, which can measure the MFR of a thermal-sensitive polymer material. An MFI device normally comprises load weights, a piston, a heated barrel with a die, a cutter system, and a scale. Usually, the procedure of measuring MFR acts by these steps: first, heat up the barrel to the desired temperature; second, add the polymer sample into the heated barrel and wait for a certain time until the sample melts, i.e., preheat time; third, put the weight on the top of the piston then after a certain period of time, measure the mass of the extrudate forced to pass through the die. Before and after the tests, the barrel and die should be cleaned to ensure no contamination and repeatability of the tests, which usually follow ASTM or ISO standards to define timings, temperatures, weight, and dimensions of the main MFI components [60]. Among the common commercialized MFI systems, some of them are cumbersome to operate and are not automated. For example, the MFI products from MRCLAB need operators to put the weight on the top of the instrument and count down the time [76]. Normally the operator needs to collect the samples and weigh them afterward, such as for many melt flow indexers on AliExpress [75]. To address this issue, the open-source MFI designed in this article was developed to be mostly automated. In the proposed design, the OS MFI can apply loads automatically via the DC motor, cut the extruded material, and weigh it automatically.

To fulfill the functionality of the MFI, the system here described relies on mechanics, electronics, and free and OS software, all of which are available on the Open Source Framework [77]. The BOM for the make, mechanical, and electronical parts are included in Appendix A. The mechanical components are composed of aluminum extrusion profiles, 3D printed parts, and fasteners. The overall structure is a vertical frame that holds a cylinder, which works as the heated barrel to melt the sample materials. In the electronic part, the instrument is controlled by a Teensy 4.0 board [78],

 doi:10.20944/preprints202409.2305.v1

and temperature control, motor, and digital scale systems are integrated into one control system. The whole process will be controlled by the code upload to the teensy board to make it easy to operate and automatic. The cutter on the MFI device can cut the extrusions at set intervals to automatize the extrudate collection from the die, and the digital scale can weigh them and record data. Finally, the device designs are meant to be open source, hence digitally replicable and low cost. All the buy components used for the hardware design are readily available on the market. Custom parts are designed to be quickly produced with low-cost desktop-size FFF 3D printers and commercial filament feedstock, i.e., PETG and polycarbonate (PC). The structure of the frame is designed to optimize material usage, hence, to be produced with less material and require a limited amount of buy components. For this reason, far less machining is needed than conventional MFI devices, further reducing costs.

2.1. Mechanical System

The framework consists of two 20x20 mm aluminum profiles, 75 mm and 30 mm long, respectively, and some 3D printed parts. This framework connects the different subassemblies together and keeps the whole structure steady. Compared to commercial MFI products, this design uses a stepper motor as the weight on the top of the piston. With the linear rail, the shaft of the motor can move up and down on the same track, which helps decrease the vibration on the motor rod. The piston is made of a piston head and a piston rod, and the piston head has a multi-layered structure, which consists of two nuts, one O-ring, and one washer. The O-ring keeps the piston head from leaking. The piston rod is a threaded steel rod, it allows the piston head to screw on it. There is a button shape load cell between the motor shaft and piston rod, which can measure the pressure so that there is a feedback loop for the motor to keep the same pressure. The barrel for heating up samples is a 304 stainless steel pipe, which can be found easily on the market. A copper cap with a hole is then added to the barrel to act as the die. A PC insulation housing with heat insulation cotton material covers the whole heated barrel to ensure heat stability. Below it, there is a servo motor equipped with a blade that acts as the cutter for the material samples to be weighted. The overall design of the mechanical system of the MFI device is shown in Figure 1, and the BOM is visible in Appendix A.

 doi:10.20944/preprints202409.2305.v1

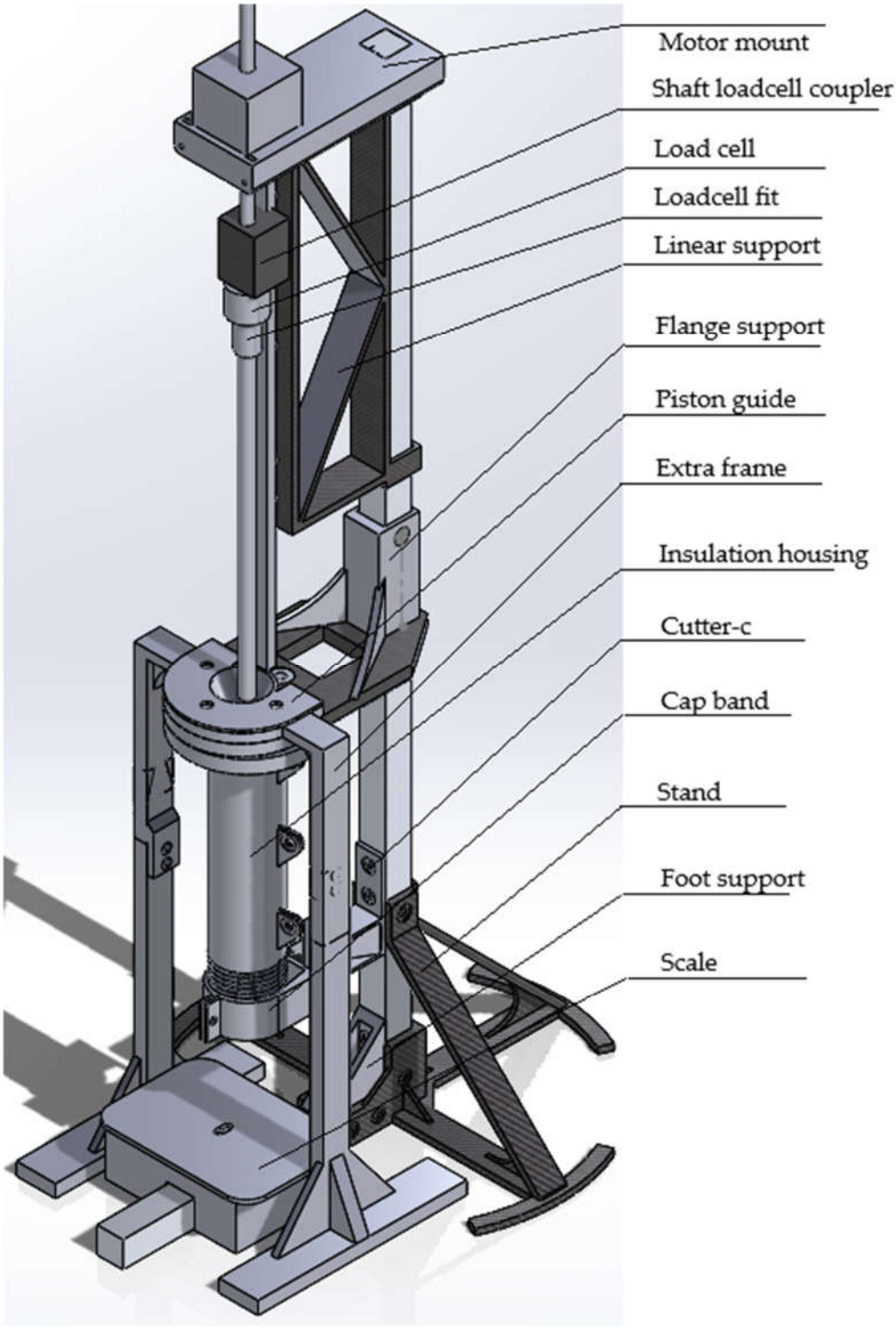

Figure 1. Overall hardware structure of the OS MFI device.

2.2. Electronics

To control the system, there is a Teensy 4.0 board that acts as the control board. The control system, as shown in Figure 2, can be divided into two main parts, which are the heating system and the motor force control system. As mentioned above, there is a feedback loop for the motor. When the force does not reach the desired value, the current of the motor will increase so that the torque output of the motor will increase. PID control is applied to the heating control system. All the terms in the PID control system need to be adjusted according to different situations. For example, if the overshot is too high, then it can be improved by reducing the portion term. This system itself runs

 doi:10.20944/preprints202409.2305.v1

automatically, but all the input parameters like time, temperature and pressure need to be input manually in the code or firmware. There are two modes in the code, which are auto mode and manual mode. Manual mode is meant for adjusting the position of the piston head, and cleaning procedure after measuring process.

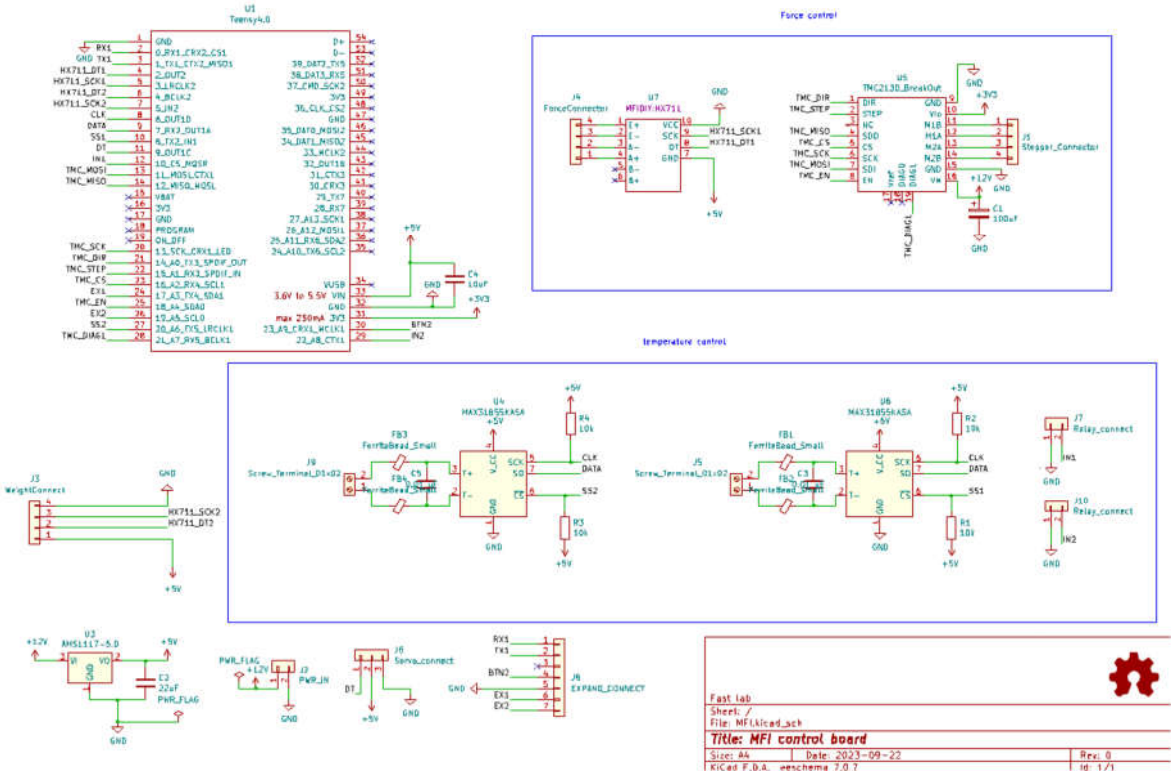

Figure 2. Electronic schematic of the OS MFI device.

2.3. Testing and Validation

2.3.1. Calibration Process

Before testing or validation, the tester needs to be calibrated to ensure precise testing results. There are three subsystems that need to be calibrated: 1) the force control system, 2) the temperature control system, and 3) the cutter system.

In the force control system, the load cell between the motor rod and the piston needs calibration. It can be calibrated by using a known weight, and a calibration factor can be obtained after this process. The detailed operation instructions are included in the calibration code in OSF [77]. To perform the calibration correctly, a 3D printed calibration part should be applied (Figure 3 and Appendix A, part 19). The calibration factor may change after installation and needs to be checked before testing.

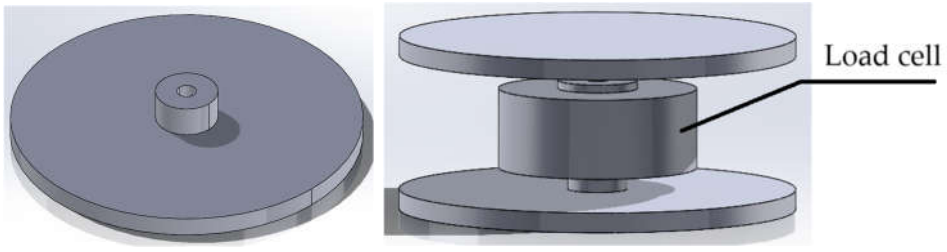

Figure 3. Load cell calibration part (left) [79], the assembly (right).

 doi:10.20944/preprints202409.2305.v1

For the temperature control system, the two heating elements of the OS MFI system need to be calibrated to ensure the temperature is the same in the heated barrel and the cap. It can be done by using another temperature sensor as a reference, for example, an additional thermocouple previously calibrated. The temperature is stable in the heated barrel of the OS MFI system, but there is about a 5-degree gap between the inside and outside of the cap, requiring an adjustment of the temperature setpoint on the cap. This fact may be due to different heat loss rates of the parts or insulation issues on the cap, making calibration important to reach stable and precise temperature values.

The movement of the cutter system can be adjusted in the code in terms of cutting time interval or moving range of the tool. As the position of the blade may affect the cutter performance, it needs to be adjusted before the testing process manually. For instance, it can be adjusted by moving the cutter-fix part until touching the bottom of the cap with the blade.

2.3.2. Validation Process

The operational instructions of the OS MFI device are detailed in Appendix B. To validate the use of the OS MFI, a series of experiments was designed to compare the measurement results of the OS MFI system with a commercial product available on the market. Compared to the commercial versions, the design of the proposed OS MFI device has some differences, e.g., the diameter and length of the heated barrel, from the specifications in the standardization documents, such as ISO-1133 [80] and ASTM D1238 [81].

The design of experiments follows the principles of a controlled variable experiment. Except for the difference in testing systems, all other experimental conditions, such as the testing parameters and the materials, are kept consistent. To compare the developed MFI with its commercial counterpart, an Instron CEAST MF20 machine (Instron, Norwood, MA, US), located at the LRGP laboratory in Nancy, France, was utilized following the ASTM D1238 [81] standard.

Materials were obtained from various sources, including virgin pellets, recycled plastic waste, blend combinations with compatibilizers, and shredded 3D printing waste from the laboratory. They were dried at 60 °C for two days before the test. Virgin PLA pellets were supplied by NatureWorks (Savage, MN, USA) with a specific gravity of 1.24 g/cc. Recycled HDPE/PET flake blends were obtained from water bottles coming from the French brand Cristaline and processed at the ERPI laboratory in Nancy, France. This material comprised 10 wt% HDPE (cap) and 90 wt% PET (body), hereinafter called rPET90/rHDPE10. The same recycled material was tested with an addition of 10 wt% styrene-ethylene/butylene-styrene block copolymer (SEBS) G-1652 containing approximately 30 wt% polystyrene units (rPET90/rHDPE10/10SEBS), kindly donated by Kraton Polymers (Almere, Netherlands). Additionally, recycled PETG from shredded 3D printing waste at the FAST laboratory was tested. The shredded waste parts were originally fabricated using virgin PETG filaments provided by Polymaker (Shanghai, China).

To ensure the reliability and repeatability of the process, the analysis was performed on three samples of approximately 5 g for the commercial and 10 g for the developed OS MFI. The materials were tested at temperatures of 190 °C for virgin PLA, 220°C, 230 °C, 240°C for recycled PETG, and 255 °C for rPET90/rHDPE10 and rPET90/rHDPE10/10SEBS, using a 2.16 kg weight. The measurement procedure can be found in Appendix B.

3. Results

Table 1 presents the results obtained from virgin PLA, rPET90/rHDPE10, rPET90/rHDPE10/10SEBS, and recycled PETG using both commercial and OS machines. The results were then compared with the data sheets of the virgin materials for PLA and PETG filament, as well as values from the literature on 3D printed PLA [39,56,82,83], PETG [84–86], HDPE and PET [70,87]. It can be observed that the MFI of PLA assessed with the commercial device corresponds to 6 g/10min and a relative standard deviation of ~13%, demonstrating both the precision and accuracy of the commercial machine. In contrast, the OS machine exhibited a 15% value decrease compared to the commercial machine despite a better relative standard deviation, i.e., ~5% when the preheating time is 10 minutes, and a comparable value with ~19% standard deviation when the preheating time is

 doi:10.20944/preprints202409.2305.v1

13.5 minutes. The results are comparable with the state-of-the-art, which shows significant variations in the MFI values, also influenced by the different feedstock batch and grade, i.e., molecular weight and additives of the specific formulation. For instance, Wang et al. obtained MFI of ~4.3 and ~11.1 g/10min at 190 °C and 210 °C [56], whereas Nasir et al. reached ~11 g/10min at 190°C [83]. Tian et al. reported values of ~2 g/10min at 180 °C, which significantly increased at 240 °C [39]. In general, MFI values of 3D printed PLA range between 6 and 10 g/10min [82], confirming the reliability of the results obtained from the commercial and OS MFI devices.

Regarding PETG, the filament datasheet indicated MFI values of 3.9 g/10min and 10.8 g/10min at 220 and 240 °C, respectively. The value obtained with the commercial machine is 9 g/10min at 230 °C with a relative standard deviation of ~6%. This MFI value is within the range of the commercial virgin filament [88], suggesting that the 3D printing and shredding processes do not significantly impact material degradation. Similarly, the MFI obtained with the OS machine fell between the two values from the datasheet, showing a decrease of ~23% compared to the commercial machine. As for PLA tests with the OS MFI, the values are in line with the state-of-the-art, where results of ~10.5 g/10min have been reported at 240 °C [84]. To ensure comparability with the datasheet, the tests were also conducted at 240°C. The MFI recorded from the commercial machine was 14.3 g/10 min, while similar values were found for the OS MFI, with a value of 13.6 g/10 min. This slight increase in MFI may be attributed to minor degradation of the material during the process. The test conducted at 220°C yielded values of 6.5 g/10 min and 4.2 g/10 min for the commercial and OS MFI, respectively, with this decrease possibly attributed to inherent variability in the testing process; significant variability in the results was also reported for PETG. For example, Vijayasankar et al. reported an MFI of ~20 g/10 min at the same temperature [85]. Kotomin et al. compared the MFI values of PETG from different temperatures, obtaining ~15 g/10min at 240°C and more than 30 g/10min at 250 °C [86]. For this reason, the values from the measurements with the commercial and OS devices can be considered reliable, confirming the validity of the OS machine.

The HDPE/PET blends derived from the plastic bottle waste stream showed MFI values of 34.5 g/10min without compatibilizer (rPET90/rHDPE10) and 31.1 g/10min with compatibilizer (rPET90/rHDPE10/10SEBS) when tested with the commercial device. Compared with the OS device, it can be observed that MFI is ~15% higher and ~34% lower with compatibilizer and without compatibilizer, respectively. Considering the lack of direct comparison from the state-of-the-art, some considerations can be made by checking the MFI values reported for HDPE and PET. Previous works obtained MFI values ranging between 3.5 and 40g/10min for PET, showing a significant variability given by the pre-heating conditions [87,89,90]. HDPE MFI values from the literature also exhibit the same trend [59]. Nevertheless, the results from the commercial and OS MFI devices are comparable, indicating the reliability of the OS machine in testing novel material compositions and plastic blends.

Table 1. MFI test parameters and results (mean values and standard deviations) of virgin PLA (vPLA), recycled PETG (rPETG), rPET90/rHDPE10, and rPET90/rHDPE10/SEBS10 obtained with the commercial and OS MFI devices.

Material	Weight (g)		Preheat time (s)		Temperature (C°)	MFI (g/10min)		
	Commercial	OS	Commercial	OS		Datasheet	Commercial	OS
vPLA	5	10	300	600	190	6.0 [91]	6.0 ± 0.8	5.1 ± 0.3
	5	10	300	810	190	6.0	6.0 ± 0.8	6.0 ± 1.2
rPETG	5	10	300	600	240	10.8 [88]	14. 3± 1.5	13.6 ± 2.7
	5	10	300	600	230	-	9.0 ± 0.6	6.9 ± 0.9
	5	10	300	600	220	3.9	6.5 ± 0.8	4.2±0.5
rPET90/rHDPE10	5	10	300	600	255	-	34.5 ± 4.3	18.3 ± 6.0
rPET90/rHDPE10/SEBS10	5	10	300	600	255	-	31.1 ± 4.3	36.9 ± 15.4

 doi:10.20944/preprints202409.2305.v1

When dealing with data from the OS MFI device, only the last ten sets of data are accepted. According to Figure 4, there is a clear increasing trend of extrusion weight through time for PLA, and all the tested materials show a similar trend when using the OS MFI device. However, the results for commercial equipment do not show this trend. One factor that can cause this phenomenon is the difference between the real temperature inside the die and the nominal one at the beginning of measurement. It may be due to insufficient insulation on the bottom of the cap, which can cause heat loss and less thermal control. The difference in materials between the cap and the heated barrel can also lead to differences in heat transfer, requiring a calibration step of the temperature control system (Sub-section 2.3.1). A preload process may be needed for a more precise result. For example, the first few samples flowing from the die can be discarded as part of the preload process, and the number should be determined through preliminary tests with specific materials. Due to a higher sample mess used in the OS MFI, the whole testing process may take a longer time, which can increase material degradation and affect the results.

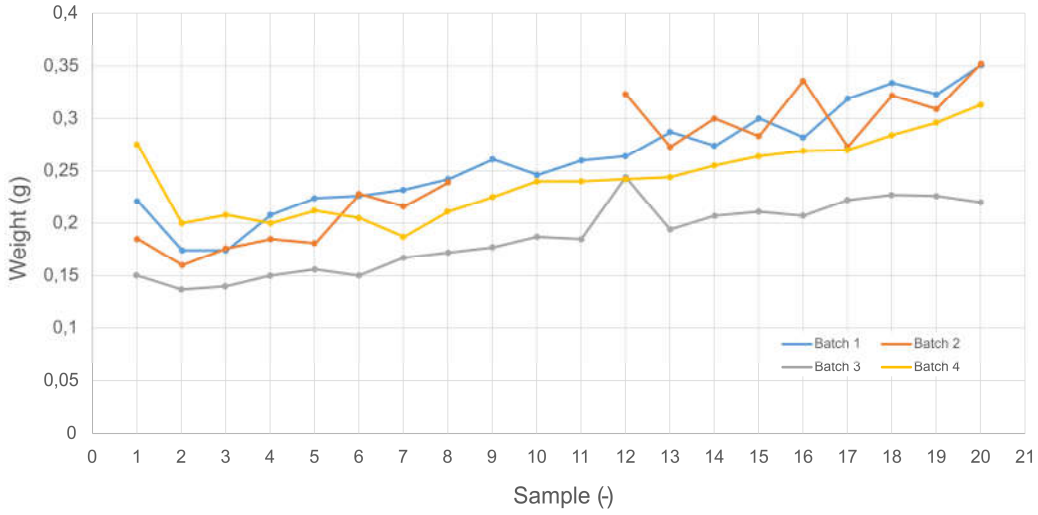

Figure 4. Virgin PLA measurement results with the OS MFI device Each sample (dots) was collected after a progressive interval of 30 s, which means 1 = 30 s, 10 = 5 min, and 20 = 10 min.

Multiple experiments were done to verify this phenomenon through OS MFI, as shown in Figure 5. Accordingly, the material is fully heated in ~8 minutes. The results show a clear linear increasing trend with the increase in pre-heating time. Therefore, it is important to keep a constant sample weight throughout the tests. Moreover, according to the standard file ISO 1133, material in flake or powder shapes should undergo a preprocess, i.e., a pressing process with a vacuum pressing tool to evacuate air in samples. This step will reduce the degradation of material caused by oxygen. This fact also explains the severe degradation shown by the rPET90/rHDPE10 measurements.

Overall, as shown in Figure 6, both systems showed similar measurement precision and were capable of stable operation within a standard deviation of ~5-20%. Although calibration is required, the results indicate that the OS MFI system can measure the MFI of different materials with precision comparable to commercial MFI devices. The data obtained from the OS MFI system can be useful to observe and make relative comparisons of different melt materials or temperatures, outlining the overall behaviors of each processed feedstock. Additionally, the study demonstrated the use of the OS MFI with different thermoplastic materials, either virgin or recycled. Compared to the PLA test data, there is a larger difference between the weight of extrudates made of PETG and HDPE/PET blends. This phenomenon could be due to the substantial differences in shape and size of the shredded PETG and HDPE/PET blends, e.g., different granulometries and dimensional ratios between pellets and shredded flakes, leading to the formation of voids during extrusion, thereby affecting the measurement results and increasing their variability [80,92].

Preprints.org (www.preprints.org) | NOT PEER-REVIEWED | Posted: 29 September 2024 doi:10.20944/preprints202409.2305.v1

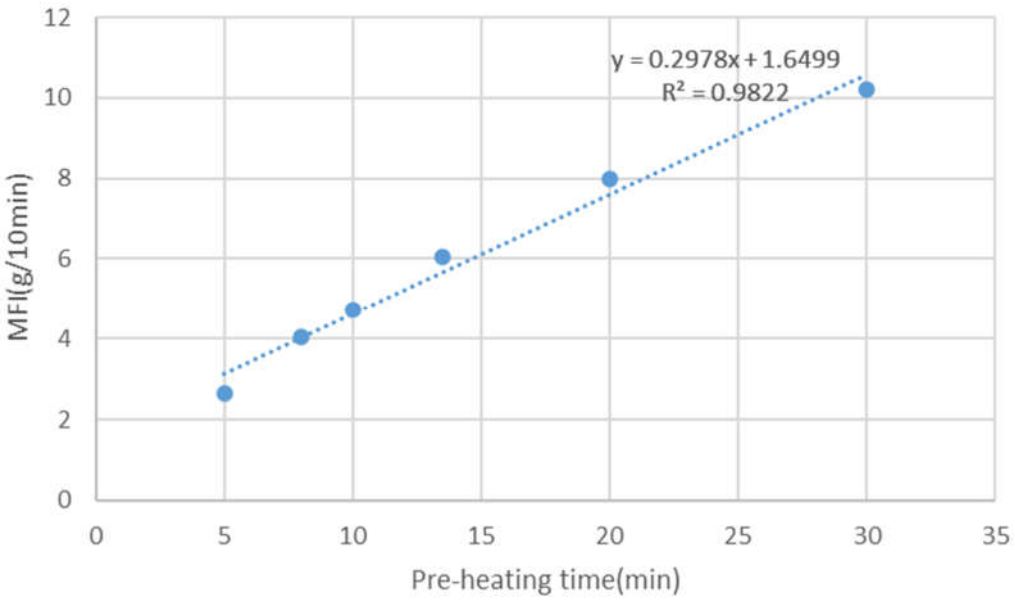

Figure 5. Virgin PLA MFI values changing through different pre-heating times from the tests with the OS MFI device.

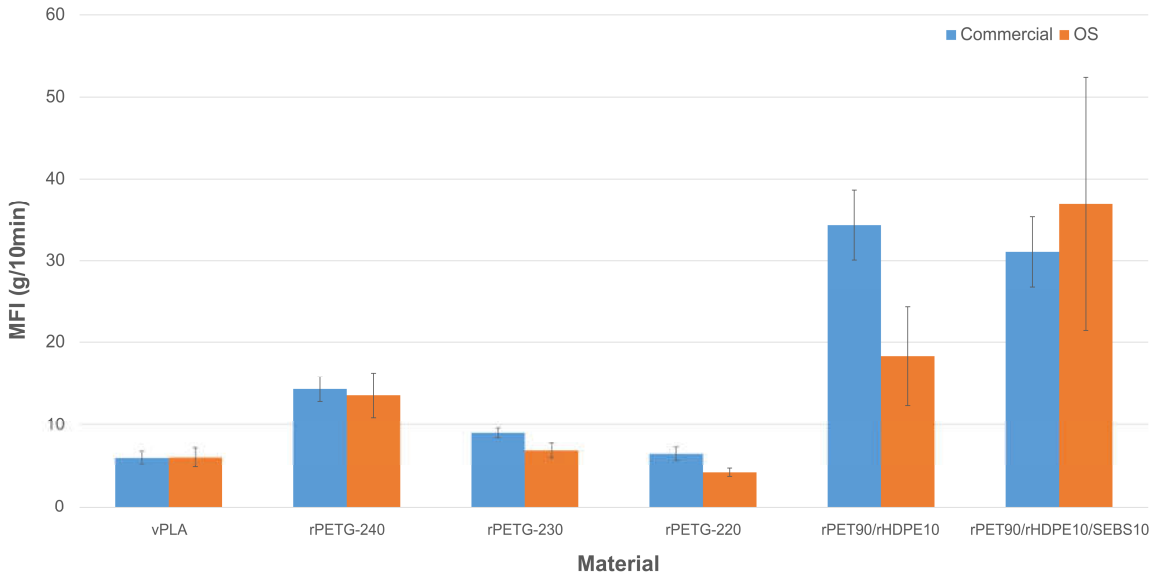

Figure 6. MFI measurement results of virgin PLA (vPLA), recycled PETG (rPETG), rPET90/rHDPE10, and rPET90/rHDPE10/SEBS10 obtained with the commercial equipment (left side bars) and OS MFI devices (right side bars).

4. Discussion

At the community scale, developing a distributed recycling process required the whole value chain to be adequate, from waste-to-product. In that sense, qualifying the plastic waste stock in a quick and efficient manner represents a challenge for the implementation of this process in a particular territory. The melt flow index MFI measurement represents a potential means to resolve this issue.

The OS MFI device developed in this research offers an accessible and low-cost way to rapidly assess the flowability and printability of recycled thermoplastic materials and blends. To validate the accuracy of the OS machine, a comparison was conducted with a commercial MFI device and the state-of-the-art. The results show differences with both the OS MFI system and commercial device

 doi:10.20944/preprints202409.2305.v1

compared to the datasheet and the literature. The measurement of the MFI can be significantly affected by the feedstock grade, e.g., molecular weight and specific additives, but also by different parameters such as temperature, load weight, the diameter of the die, the diameter of the barrel, and their cleanness [50,63], as well as the heat transfer conditions in the whole device itself. For instance, increasing the testing temperature of 10 °C can lead to a two- or three-fold increase in the MFI values, such as for PETG feedstock [86]. Moreover, as shown in the results part (Section 3), the pre-heating conditions can also significantly modify the results, e.g., with differences of one order of magnitude [87]. Despite equal temperatures and load weights, the diameters of the barrel and die might impact the measurements, as well as the properties of the materials used for these components, e.g., different heat capacities and specific heats [56]. Changes in these factors reasonably explain the differences in the test results between OS and commercial MFI devices. Likewise, inconsistencies can be found regarding the MFI test results in the literature, even for similar materials used from variability in material grade. For instance, Singh et al. reported an increase in the MFI of recycled ABS [55], whereas other works demonstrated a decrease in the MFI of the same material [72,73]. Again, these contradictory results highlight the variability in MFI values, which may be influenced by differences in experimental conditions, material processing, measurement techniques, or the measuring equipment used in these studies, as well as different feedstock grades and tested batches. Furthermore, according to Rides et al., MFI measurement has larger differences between different laboratories [64], confirming the variability in the equipment conditions, environment, e.g., room humidity, and setup, especially for polar and relatively polar materials.

Providing the whole code for the OS MFI could help overcome this challenge, ensuring that any research lab, community makerspace, or other DRAM facility could use nearly identical systems. Compared to standard commercial MFI devices, the OS MFI developed in this study utilizes a DC motor to apply the load weight, which can impact the measurements, as load weight is a critical parameter. From a user perspective, this feature can simplify the operation and enhance the safety of the measurement process, making it more accessible and repeatable in DRAM contexts. It is important to highlight that MFI is a valuable tool for the rapid assessment of the flowability and potential printability of materials. For more detailed and scientifically rigorous results, however, comprehensive rheological analysis using rheometers should be conducted even when using commercial MFI devices. These tests can help better understand the behavior of the molten material under high shearing, such as in 3D printer extruders. Furthermore, MFI can not only be used in DRAM contexts or recycling activities but also in laboratory environments [94]. This choice can help make research more affordable and reliable because this characterization can support the fine-tuning of 3D printing parameters with novel material formulations, helping to ensure extrudate consistency and, hence, improving the technical properties of the final parts, e.g., achieving better mechanical properties by reducing voids and defects from extrusion inconsistencies.

There are limitations of the OS MFI device that need future work. Currently, cleaning procedures are labor intensive. The cap needs to be disassembled to clean it from the inside, requiring the disconnection of the band heater and thermocouple. Creating or identifying specialized cleaning tools to simplify the cleaning process could reduce the difficulty of cleaning. Furthermore, the temperature control system could be improved in accuracy as it currently shows variations of ~2 °C. Although there are two heating systems, the nichrome wire, and the band heater, temperature difference still exists in the MFI device, leading to different MFI values according to the specific pre-heating times (Figure 5). For example, the temperature in the die on the cap could be lower than other parts, e.g., 170 °C instead of 190 °C, affecting its accuracy. Future experiments could also consider the thread of the cap. Due to the threaded fit of the cap and the pipe (National Pipe Taper, NPT), the cap cannot thread all the way up. This constraint leaves a part of the thread exposed, and it can affect the shear force when extruding, potentially influencing the beginning of the measurements. This thread type, however, helps prevent leakage, increasing accuracy and limiting the shear force effect.

To have better accuracy, some improvements can also be made to the device. According to the previous test at 190°C, the position of the band heater significantly modifies the actual temperature in the die. If the position of the band heater is up, roughly where the bottom of the cap can be exposed,

 doi:10.20944/preprints202409.2305.v1

the temperature in the die will be 170 °C, while if the position of the band heater is down, roughly where the cap can be completely covered, the temperature will be 182 °C. This test shows that the relative position of the band heater and cap affects the temperature inside the die, showing a significant improvement after fixing the position of the band heater and the cap. These results indicate that the stability of the temperature is a key factor in getting a more accurate MFI measurement. Hence, further accuracy improvements might be made by reinforcing the insulation layer and having a more advanced temperature control system, including improved insulation, temperature sensors, or advanced temperature control algorithms. The accuracy of the digital scale and its interaction with the cutter system can also impact results. In the current OS MFI device, the weight is unevenly distributed on the scale plate, leading to potential measurement errors. Improvements in scale and cutter design can, therefore, increase accuracy. A better motor control system can also be considered in future versions of the OS MFI device. Current motor control systems are generally accurate and can introduce some errors in the pressure. Therefore, using more advanced motor control algorithms [95] can make the pressure more accurate, making the results more accurate as well. Finally, future work could include a Graphical User Interface (GUI) to make the system easier to operate and guide data interpretation and analysis, especially for non-expert users or DRAM contexts.

5. Conclusions

To address the current issues with MFI systems, a low-cost OS MFI device was developed. MFI Measurements of virgin PLA pellets, recycled PETG flakes, and HDPE/PET blends were carried out using the developed device, showing good measurement precision with a ~5-20% standard deviation. Compared to its commercial counterpart, it has a ~5-23% decrease in PLA and PETG measurements, which shows a similar trend. The OS MFI can be a valuable characterization tool for easily sorting different material feedstocks, determining their suitability for FFF/FGF 3D printing, and identifying the optimal 3D printing temperature. This study demonstrated the development and use of an OS MFI with performance comparable to its commercial counterparts. The validation test reported similar MFI values for both the commercial and OS MFI devices when using common 3D printing feedstock, i.e., virgin PLA and recycled PETG, and new polymer blend formulation from plastic waste, such as HDPE/PET blends. Some challenges remain, however, particularly in achieving consistent temperature along the heated barrel and die. Therefore, future machine versions should improve the temperature control system and connection between the cap (die) and heated barrel, optimizing the heat transfer in the whole equipment, e.g., improving insulation or changing part of the buy components selected for the current version. To enhance user-friendliness, future work can develop a graphical user interface, guided testing and analysis procedures, and accessible tutorials that enable the adjustment of test parameters, such as pre-heating, weight load speed, or automated cutting timings.

The MFI devices in the market are currently expensive. An OS MFI device can make the recycling process easier and more efficient, becoming a valuable option in different contexts, such as DRAM and laboratory environments. A more affordable and accessible version of MFI devices can help enable DRAM to become more widespread and trustable in terms of material manufacturing processing.

Author Contributions: Conceptualization, H.B. and J.M.P..; methodology, D.L., A.B., C.S.G.; software, D.L.; validation, D.L., A.B., C.S.G., A.R.; formal analysis, D.L., A.B., C.S.G., A.R., H.B, C.N., F.A.C.S. and J.M.P.; investigation, D.L., A.B., C.S.G., A.R.; resources, H.B, C.N., F.A.C.S. and J.M.P.; data curation, D.L.; writing—original draft preparation, D.L., A.B., C.S.G., A.R., and J.M.P. ; writing—review and editing, D.L., A.B., C.S.G., A.R., H.B, C.N., F.A.C.S. and J.M.P.; visualization, D.L. and A.R..; supervision, H.B, C.N., F.A.C.S. and J.M.P.; project administration, J.M.P.; funding acquisition, H.B, C.N., F.A.C.S. and J.M.P.. All authors have read and agreed to the published version of the manuscript.

Funding: This research was supported by the Thompson Endowment.

Institutional Review Board Statement: Not applicable

 doi:10.20944/preprints202409.2305.v1

Informed Consent Statement: Not applicable.

Data Availability Statement: All data and designs for this project are available: https://osf.io/68hbj/

Conflicts of Interest: The authors declare no conflict of interest.

Appendix A

The bill of materials (BOM) for the make parts is shown in Table A1. The full list with links to commercially available components can be found at https://osf.io/68hbj/ [77]. All files are licensed under GNU GPL v3.

Table A1. BOM of the make parts and files for the OS MFI device (hardware).

No.	Design file name	File type	Technology	Material
1	Stand	STL&STEP	FFF 3D printing	PETG
2	Linear support	STL&STEP	FFF 3D printing	PETG
3	Motor mount	STL&STEP	FFF 3D printing	PETG
4	Flange support	STL&STEP	FFF 3D printing	PETG
5	Loadcell fit	STL&STEP	FFF 3D printing	PETG
6	Shaft loadcell coupler	STL&STEP	FFF 3D printing	PETG
7	Cutter connector	STL&STEP	FFF 3D printing	PETG
8	Blade fix	STL&STEP	FFF 3D printing	PETG
9	Extra frame	STL&STEP	FFF 3D printing	PETG
10	Extra frame b	STL&STEP	FFF 3D printing	PETG
11	Foot support	STL&STEP	FFF 3D printing	PETG
12	Housing	STL&STEP	FFF 3D printing	PETG
13	Insulation housing	STL&STEP	FFF 3D printing	PC
14	Cap band	STL&STEP	FFF 3D printing	PC
15	Piston guide	STL&STEP	FFF 3D printing	PETG
16	Piston tip guide	STL&STEP	FFF 3D printing	PETG
17	Scale housing	STL&STEP	FFF 3D printing	PETG
18	Scale plate	STL&STEP	FFF 3D printing	PETG
19	Block	STL&STEP	FFF 3D printing	PETG
20	Calibration part	STL&STEP	FFF 3D printing	PETG
21	PCB	zip		//
22	MFI	ino		//

The make parts are listed hereinafter with a short description and a rendering preview.

Part 1 (File 1). Stand: this is the basement of the whole frame, which can hold the two aluminum profiles 90 degrees, making the whole structure vertically (Figure A1).

 doi:10.20944/preprints202409.2305.v1

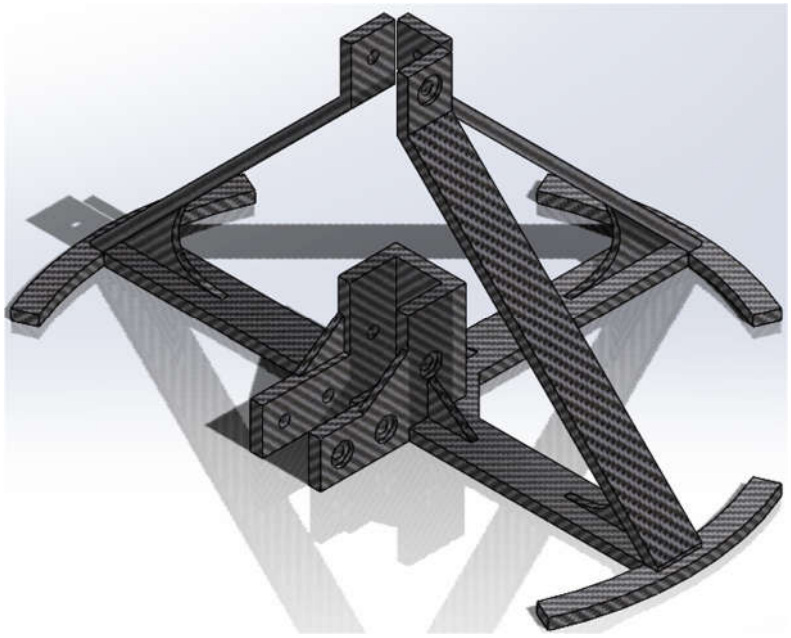

Figure A1. Part 1: Stand.

Part 2 (File 2). Linear support: this part can support the linear rail and the Motor mount part and mount the rail to the aluminum extrusion profile (Figure A2).

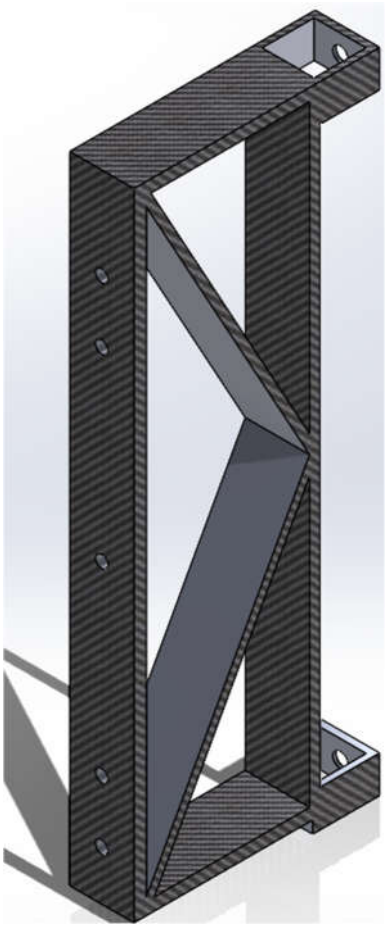

Figure A2. Linear support.

Part 3 (File 3). Motor mount: To support and mount the motor on the aluminum profile (Figure A3).

 doi:10.20944/preprints202409.2305.v1

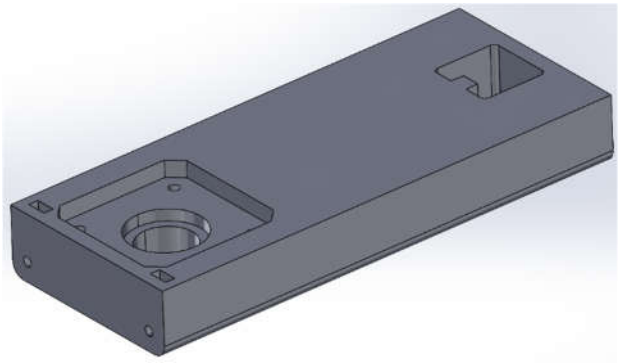

Figure A3. Motor mount.

Part 4 (File 4). Flange support: L-shaped part, with rib to increase strength (Figure A4).

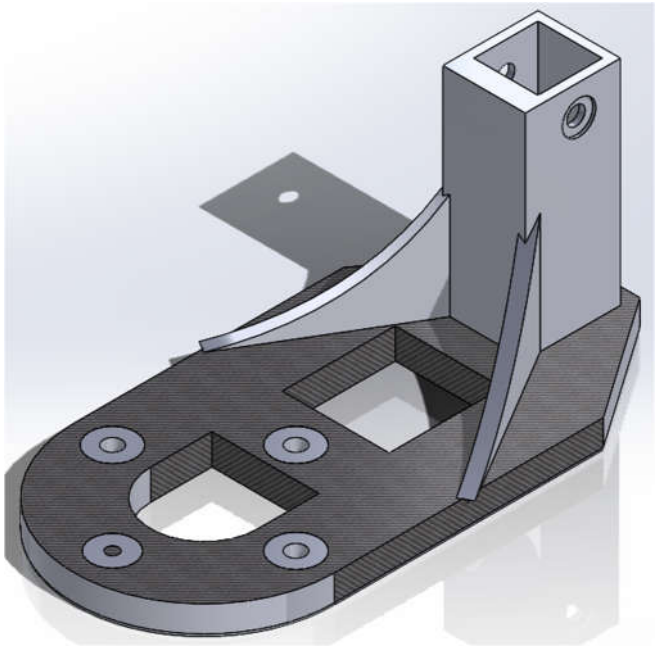

Figure A4. Flange support.

Part 5 (File 5). Loadcell fit: This is used to help connect the shaft coupler and the load cell (Figure A5, left).

Part 6 (File 6). Shaft loadcell coupler: A rectangular part with top and bottom holes. There are four blot holes, which correspond to the slide block of the linear rail. The top part is separate, which can help grip the motor shaft (Figure A5, right).

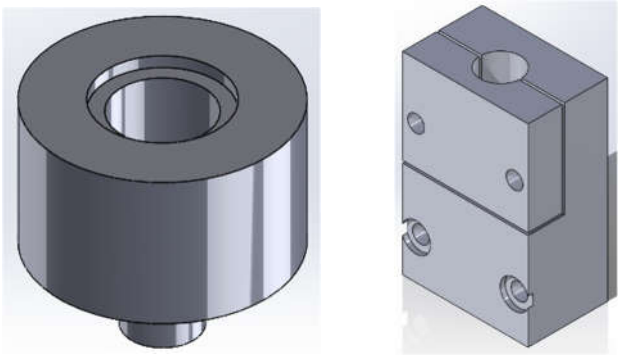

Figure A5. Loadcell fit (left), Shaft loadcell coupler (right).

 doi:10.20944/preprints202409.2305.v1

Part 7 (File 7). Cutter connector: Mount the servo motor on the aluminum extrusion profile (Figure A6, left).

Part 8 (File 8). Blade fix: Attach the blade to the servo motor (Figure A6, right).

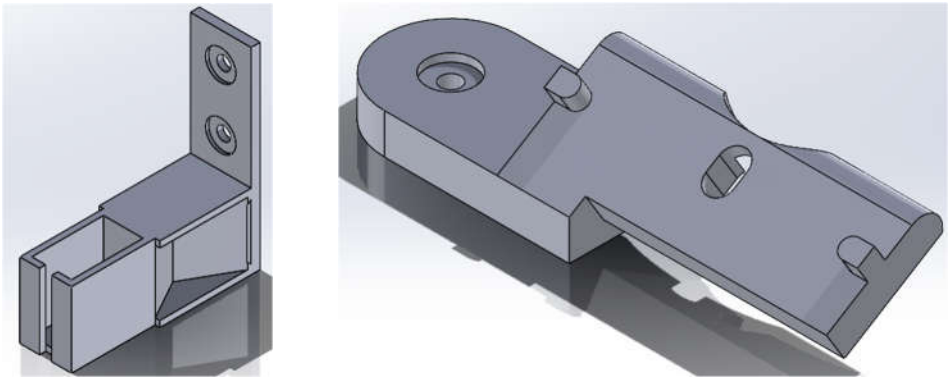

Figure A6. Cutter connector (left), blade fix (right).

Part 9 (File 9). Extra frame: provide extra support for the flange support so that it will not deform when the piston presses down (Figure A7, left).

Part 10 (File 10). Extra frame b: the bottom part of the extra frame (Figure A7, right).

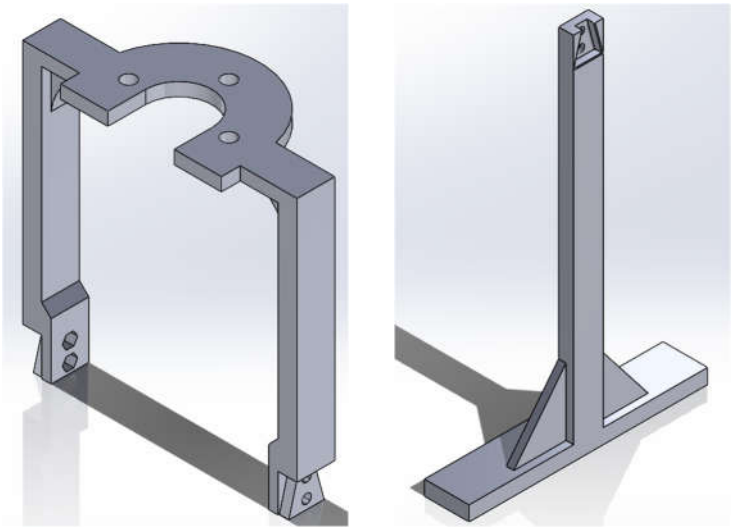

Figure A7. Extra frame (left), extra frame b (right).

Part 11 (File 11). Foot support: this part is the triangle part that goes between two aluminum extrusion profiles, so that they can keep stand vertically (Figure A8, left).

Part 12 (File 12). Housing: The shell of all electronic components (Figure A8, right).

 doi:10.20944/preprints202409.2305.v1

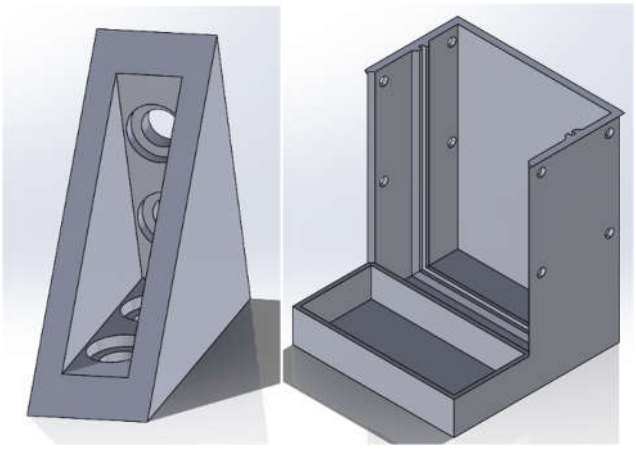

Figure A8. Foot support (left), Housing (right).

Part 13 (File 13). Insulation housing: housing for the insulation layer of the heating pipe, which helps hold insulation in place (Figure A9).

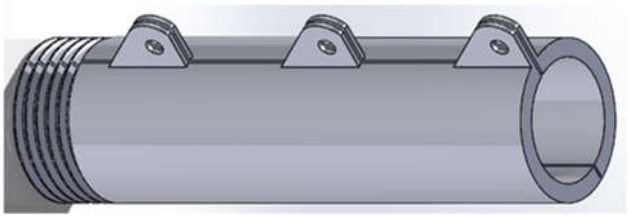

Figure A9. Insulation housing.

Part 14 (File 14). Cap band: band-shaped insulation housing for the band heater. The insulation layer is attached to this part so that the insulation can be taken off easily (Figure A10).

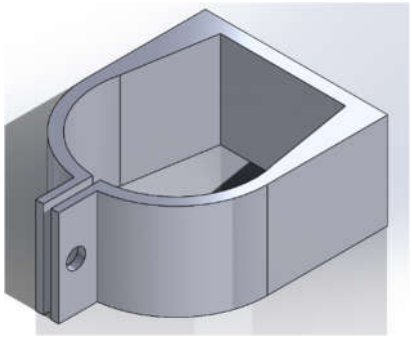

Figure A10. Cap band.

Part 15 (File 15). Piston guide: helps guide the piston insert the pipe. It also works as a fuel when adding materials (Figure A11, left).

Part 16 (File 16). Piston tip guide: A small cap for the piston tip helps keep all the components of the piston tip aligned with the same center point (Figure A11, right).

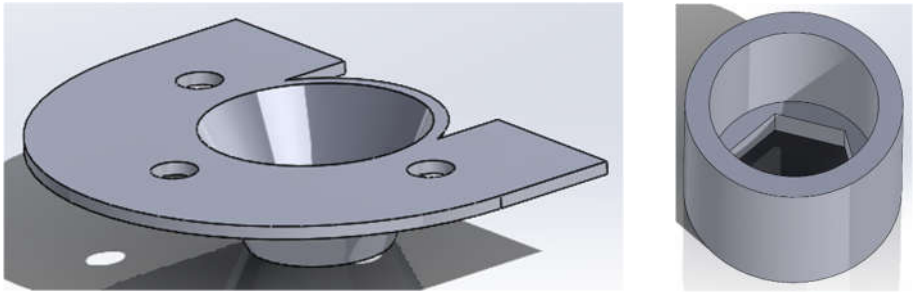

 doi:10.20944/preprints202409.2305.v1

Figure A11. Piston guide (left), piston tip guide (right).

Part 17 (File 17). Scale housing: housing for all the scale components. The scale is apart from the main body of the MFI device to avoid vibration (Figure A12, left).

Part 18 (File 18). Scale plate: a plate that can hold extrusions of the MFI (Figure A12, right).

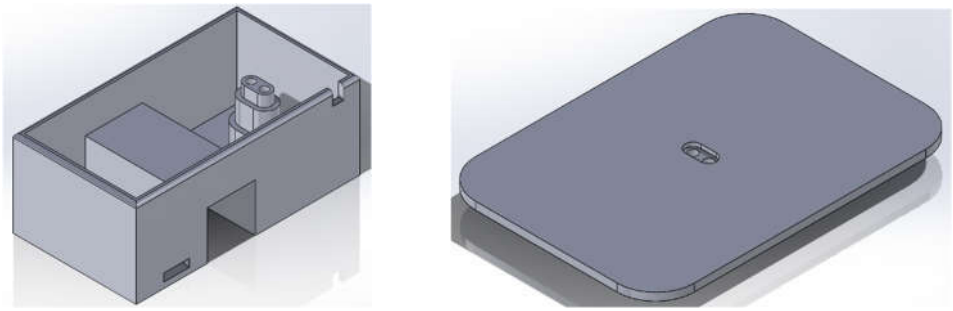

Figure A12. Scale housing (left), scale plate (right).

Part 19 (File 20). A calibration tool for the button load cell. Screw the thread on the load cell to the corresponding hole on this part.

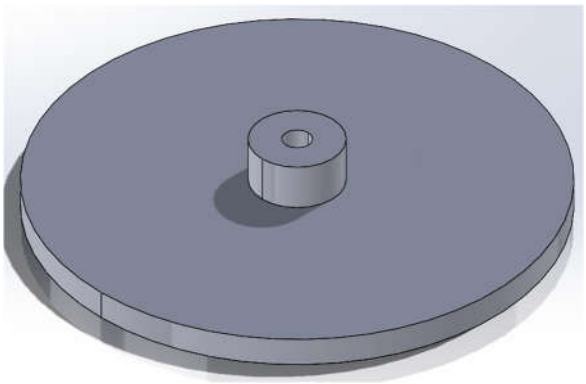

Figure A13. Calibration part.

The BOM for the electronic components is shown in Table A2, whereas the BOM of the mechanical components is visible in Table A3.

Table A2. BOM of electronic components.

No.	Name	Model number	Quantity	Cost per unit (CAD)	Source
1	PCB		1	10.00	JLCPCB
2	Control board	Teensy board 4.0	1	23.80	Teensy.com
3	Motor driver	TMC2130	1	10.0	Amazon
4	Amplifier	HX711	2	6.00	Amazon
5	ADC	MAX31855KASA	1	12.66	Digikey
6	LDO regulator	AMS1117	1	0.85	Digikey
7	Force sensor	DYMH-103	1	70.42	AliExpress
8	Loadcell	100 g	1	10.79	Amazon
9	SMD Resistor	10 k	2	0.15	Digikey
10	Capacitors c1	100 uF	1	0.48	Digikey
11	Capacitors c2	22 uF	1	0.21	Digikey
12	Capacitors c3	0.01 uF	1	0.14	Digikey
13	Capacitors c4	10 uF	1	0.14	Digikey

 doi:10.20944/preprints202409.2305.v1

14	Ferrite Beads	FERRITE BEAD 120 OHM 0603 1LN	2	0.18	Digikey
15	Thermocouple	240-080	1	15.80	Digikey
16	Connecters		8	0.10	Amazon
17	Motor	Nema 17 Non-captive Linear stepper motor	1	25.84	AliExpress
18	Servomotor		1	2.90	Amazon
19	Power supply	110v AC to 12V DC	1	22.88	Amazon
20	Relay module	12V	1	1.90	Amazon
21	Wires	Jump wires	10	0.10	Amazon
22	High temperature-resist wires	Awclub Mica	0.164 ft	0.75/ft	Amazon
23	High temperature-resist connectors	O Type and U Type	8	0.05	Amazon
24	Nichrome wire	50′ nichrome 80 wire	1	9.47	Master wire supply
25	Band heater	12V 40W	1	20.00	Filastruder

Table A3. BOM of mechanical components.

No.	Name	Model number	Quantity	Cost per unit (CAD)	Source	Material
1	Bolts b1	M6-5mm	19	0.10	Amazon	Steel
2	Bolts b2	M3-20mm	8	0.10	Amazon	Steel
3	Bolts b3	M6-40mm	3	0.10	Amazon	Steel
4	Bolts b4	M2-8mm	4	0.10	Amazon	Steel
5	Bolts b5	M3-15mm	3	0.10	Amazon	Steel
6	Nuts n1	M6	3	0.24	Amazon	Steel
7	Nuts n2	M3	3	0.10	Amazon	Steel
8	Nuts n3	M2	2	0.09	Amazon	Steel
9	T-nuts t1	M6, 20x20	19	0.20	Amazon	Steel
10	Serrated Flange Lock Nut	¼ inch	1	0.80	Amazon	Steel
11	Self-lock nut	¼ inch	1		Amazon	Steel
12	Washers w1	M6	4	0.10	Amazon	Steel
13	Washer w2	M3	2	0.10	Amazon	Steel
14	Heat tube	½ inches,	1	20.00	McMaster-Carr	Steel
15	cap	½ inches, hex	1	5.00	McMaster-Carr	Copper
16	Aluminum profile a1	20x20	75 mm	0.013/mm	McMaster-Carr	Aluminum
17	Aluminum profile a2	20x20	30 mm	0.013/mm	McMaster-Carr	Aluminum
18	Linear rail	350mm	2	0.18	Amazon	Steel
19	Blade	240-080	1	15.80	McMaster-Carr	Steel
20	Piston rod	¼ inches, 12 inches length	2	1.50	Home Depot	Steel
21	O-ring	OD5/8	1	0.26	McMaster-Carr	Silicon
22	Capton tape		1	2.90	Amazon	Mixed
23	Shaft Coupler	¼ inch	1	3.00	Amazon	Steel
24	Insert Nuts	3mm	2	1.90	McMaster-Carr	Steel
25	Insulation	heat resistance cotton	1.50 mm^2	0.08/ $inch^2$	McMaster-Carr	Fiberglass

 doi:10.20944/preprints202409.2305.v1

Appendix B

Build Instructions

1.1. Mechanics

1.1.1. Step 1. Assemble the Frame

- Insert t-nut into the slot of the 1-meter aluminum profile, assemble 3D printed part motor mount on the top of the aluminum extrusion profile.
- Insert the same aluminum profile into the two holes of linear support.
- Push the linear support until it touches the motor support, then secure it to the aluminum extrusion profile with bolts and T-nuts. Attach the linear rail to the linear support with fasteners using the corresponding holes.
- Insert the aluminum profile into the 3D printed part Flange support and fix the position with bolts and t-nuts. The position depends on the length of the linear rail.
- Put the 3D printed part of the cutter connector in the right position and fix it with bolts and nuts. The position depends on the length of the heating pipe. It should allow the cutter to cut off the extrusions.
- Insert the aluminum extrusion profile into the 3D printed part Stand and fix it with fasteners.
- Attach another aluminum extrusion profile to the stand and fix the position with fasteners. Then assemble the 3D printed part foot support and make sure two aluminum extrusion profiles are vertical.

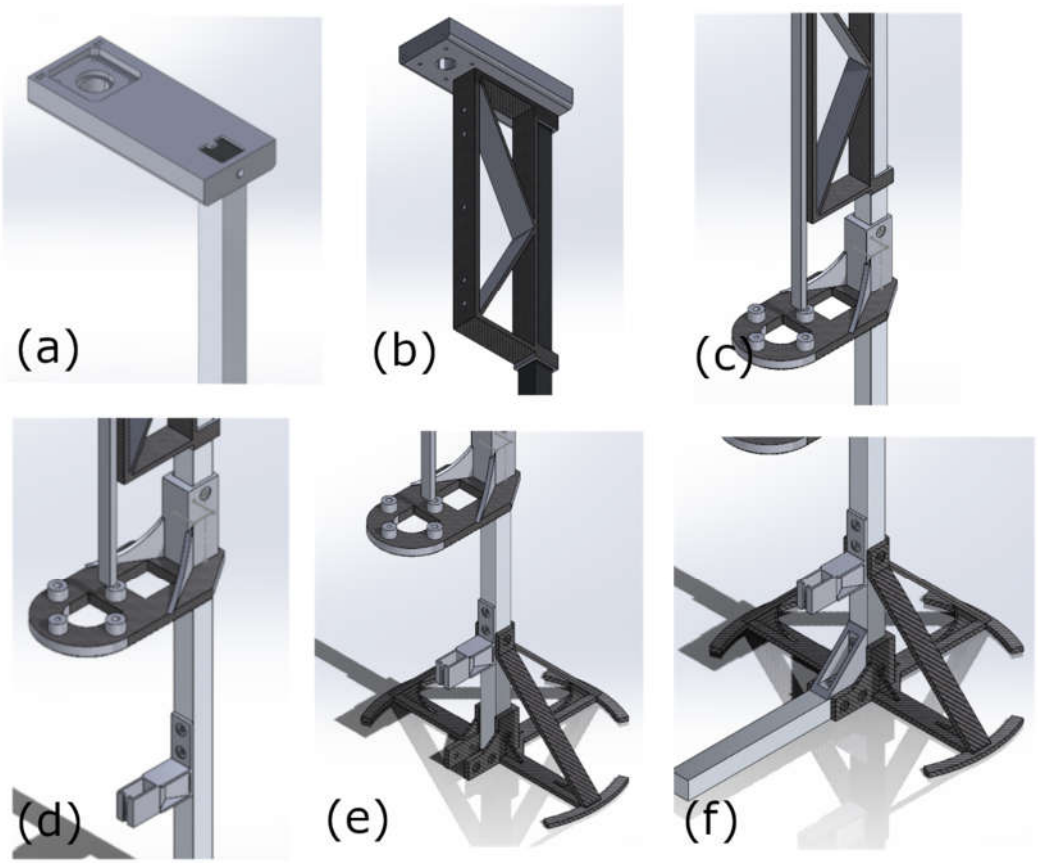

Figure B1. Frame.

1.1.2. Step 2. Piston

- Screw the ¼ inch serrated flange lock nut to the ¼-inch threaded rod and stop at 15mm away from the tip.

 doi:10.20944/preprints202409.2305.v1

- Put an O-ring on top of the nut, then put a washer on top of it.
- Screw another self-lock nut, cover it with a piston guide, and ensure that all pieces have the same center point. Use the 3D printed part Piston tip guide to make sure all the components are centered and not too tight. If the screw is too tight, the O-ring in the middle will deform, which makes it harder to insert into the heating pipe.
- Assemble the motor on the 3D printed part Motor Support.
- Connect the shaft of the motor to the shaft loadcell coupler.
- Screw the Loadcell fit into the Shaft loadcell coupler, then install it on the slide block of the linear rail.
- Screw the insert nut into the 3D printed part loadcell fit, connect the loadcell fit and the button loadcell, then screw the button loadcell to the shaft loadcell coupler.
- Connect the shaft coupler to loadcell fit.
- Connect the piston rod with the shaft coupler.

Figure B2. Piston tip.

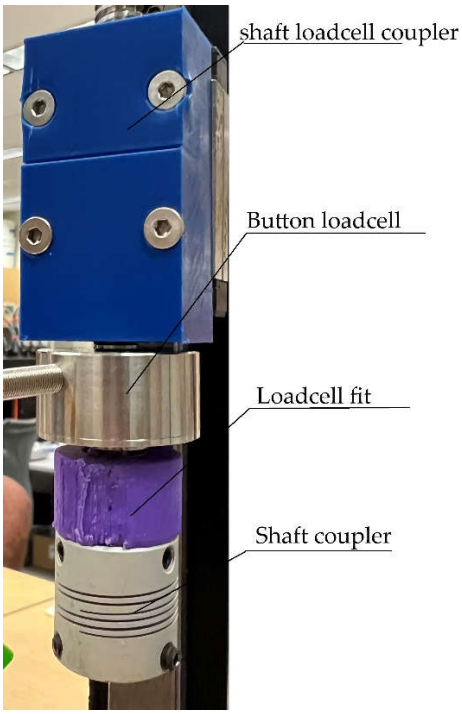

Figure B3. Coupler connection.

 doi:10.20944/preprints202409.2305.v1

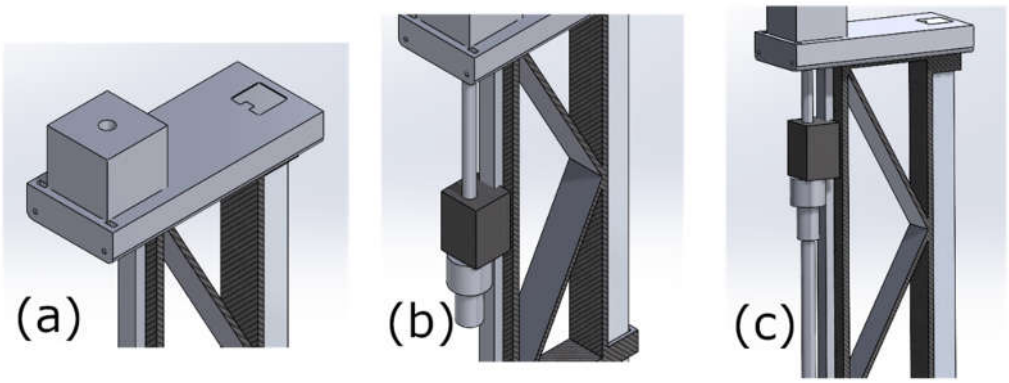

Figure B4. Piston assembling step.

1.1.3. Step 3. Heating Pipe

- Cover the whole pipe with high-temperature-resistant tape (Kapton Tape).
- Wind Nichrome wire around the iron pipe as required, ensuring the nichrome wire has sufficient resistance to at least meet the maximum current requirements of the relay. The nichrome wires must not touch each other to prevent short-circuiting or excessive heat generation at the contact points. After winding, wrap high-temperature tape around the outside of the resistance wire to achieve insulation.
- Tape the thermocouple to the outside of the resistance wire.
- Cover the pipe with heat insulation material, such as fiberglass. Cover the fiberglass layer with Kapton tape so that it can keep on the pipe.
- Cover the insulation layer with 3D printed housing (insulation housing).
- Drill a 2 mm hole in the center of the cap.
- Insert the cap in the band heater.
- Tighten the screw on the band heater.
- Cover the band heater with a 3D printed insulation cap band.
- Screw the cap on one end of the pipe.
- Attach the flange and insulation pad to the 3D printed part of the flange support with bolts and nuts. The insulation pad should be between the flange and the flange support.
- Fix the extra frame and piston guide with the same bolts and nuts as the last step.
- Screw the pipe to the flange.
- Adjust the position of the blade. It should touch the bottom of the cap.

Figure B5. Heating pipe.

 doi:10.20944/preprints202409.2305.v1

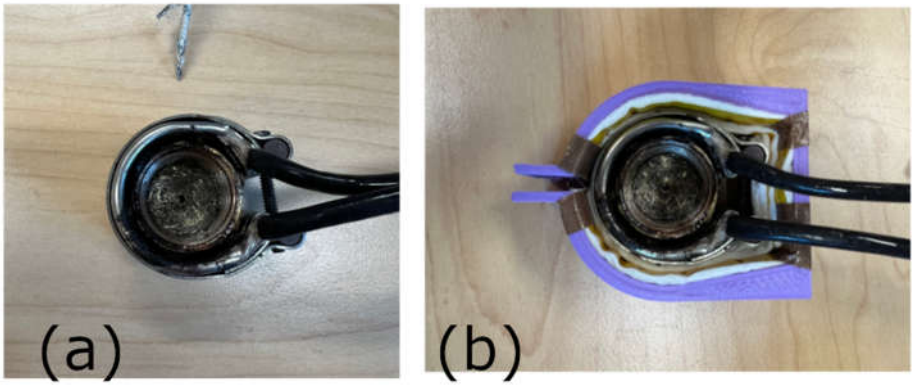

Figure B6. Cap assembly.

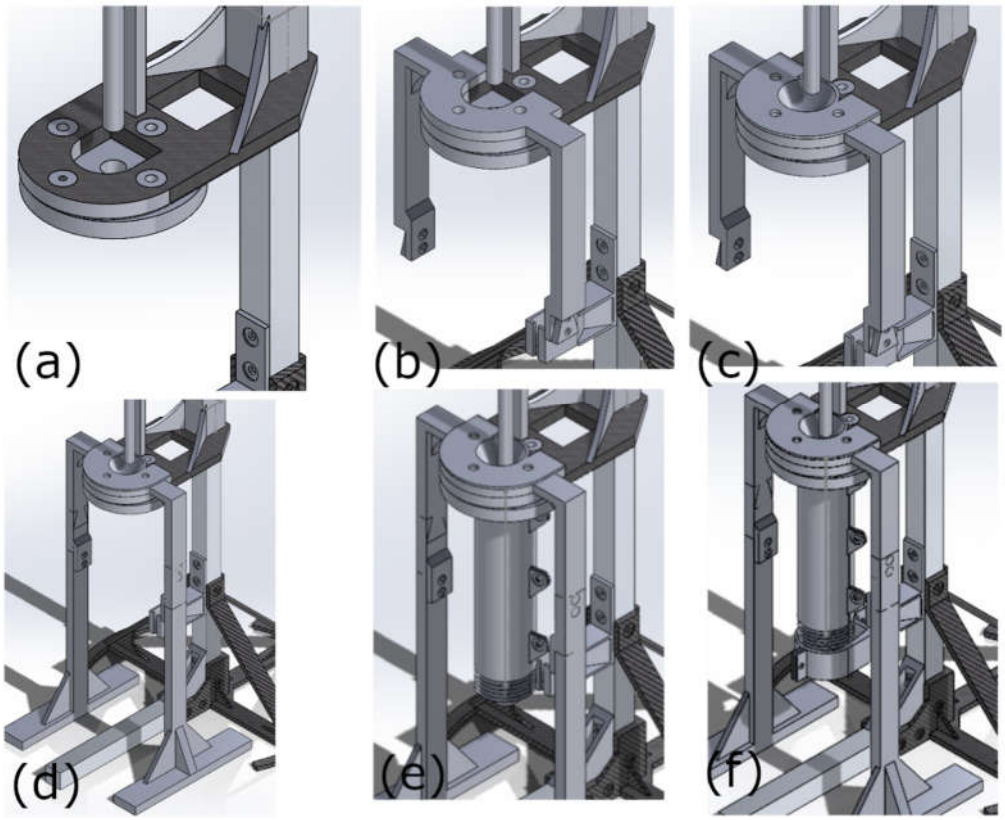

Figure B7. Assembling steps in step 3.

1.1.4. Step 4. Digital Scale

- Connect wires on the HX711 board.
- Assemble the scale platform on the load cell.
- Fix the HX711 board on the related slot in the scale housing.
- Assemble the load cell on the scale housing.
- Pull jump wires out and connect the other end to the main board.

 doi:10.20944/preprints202409.2305.v1

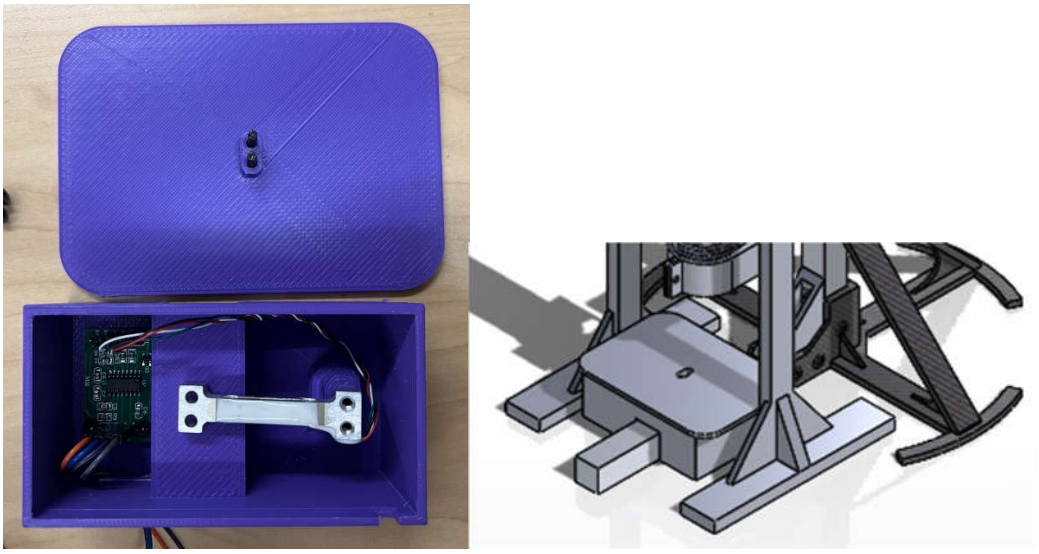

Figure B8. Scale assembly.

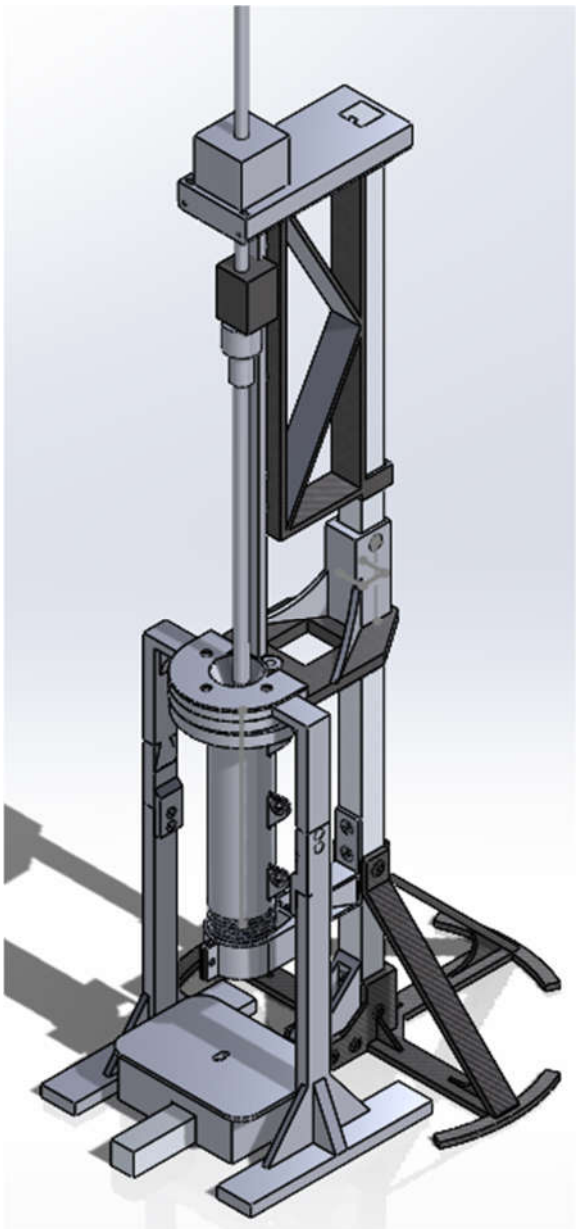

Figure B9. Overall structure.

Preprints.org (www.preprints.org) | NOT PEER-REVIEWED | Posted: 29 September 2024 doi:10.20944/preprints202409.2305.v1

1.2. Electronic

- Connect a high-temperature resistant connector to one end of the high-temperature resistant wire and connect it to the nichrome wire.
- Follow the instructions in the schematic in the Open Science Framework [77].

Operation instructions

Preparation: Humidity-sensitive materials like PETG and PLA should be dried before measurement. Get a specific weight of the material, such as 10 grams, and dry it. The drying process should follow the standard profile.

1. Connect the Teensy board with the laptop.
2. Plugin the power supply.
3. Open the .io file with Arduino IDE and download all the libraries. Setup parameters are needed, and the new firmware is uploaded to the teensy board. More detailed instructions are in the code file.
4. Open the Serial Monitor in Arduino IDE, baud rate 115200. "start" should show up in the Serial monitor.
5. Input start command monitor "a "in Message blank. The temperature will increase, and the piston will start to go down automatically after the heating-up procedure ends.
6. Fill in the samples when the temperature reaches the set point.
7. Bring down the piston using the command "d". The piston will start to go down automatically after the heating-up procedure ends.
8. Wait for the pressure to get to the set point. Record the readings after the cutter cut-off samples.
9. Clean up the barrel and the cap after the measurement is finished.

Data processing method: get at least 20 data sets, where the first X data sets should be abandoned. This fact is due to the initial temperature instability in the heated barrel and die. Only the last X sets of data should be considered for MFI measurement to achieve accurate results.

Figure B10. Operation instruction step 4.

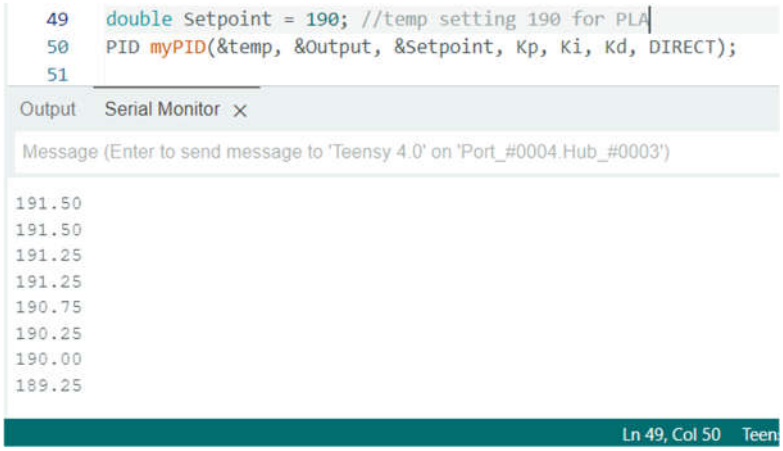

Figure B11. Operation instruction step 5.

 doi:10.20944/preprints202409.2305.v1

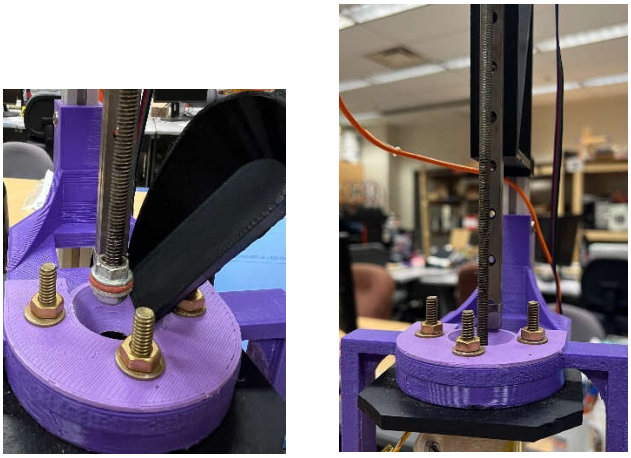

Figure B12. Operation instruction step 6 (left), step 7 (right).

Cleaning instructions

1. Go into cleaning mode by inputting the command in the Arduino IDE serial monitor to keep the temperature.
2. Dissemble the insulation band, unplug the band heater, and unscrew the cap with a clamp or heat-resistant gloves.
3. Plug the band heater back and clean the cap with cleaning tools, such as a copper brush, etc.
4. Pull out the piston and clean the piston tip with cleaning tools.
5. Clean the tube with the piston and cover the piston tip with a cotton rug or robust paper.
6. Screw the cap back after the cleaning process.

References

1. Statista Research Department, "Global plastic production 1950-2021," Statista. Accessed: May 08, 2023. [Online]. Available: https://www.statista.com/statistics/282732/global-production-of-plastics-since-1950/
2. G. Maitlo *et al.*, "Plastic Waste Recycling, Applications, and Future Prospects for a Sustainable Environment," *Sustainability*, vol. 14, no. 18, Art. no. 18, Jan. 2022, doi: 10.3390/su141811637.
3. A. L. Andrady, Ed., *Plastics and the Environment*, 1st ed. Wiley, 2003. doi: 10.1002/0471721557.
4. C. J. Moore, "Synthetic polymers in the marine environment: A rapidly increasing, long-term threat," *Environ. Res.*, vol. 108, no. 2, pp. 131–139, Oct. 2008, doi: 10.1016/j.envres.2008.07.025.
5. S. Bejgarn, M. MacLeod, C. Bogdal, and M. Breitholtz, "Toxicity of leachate from weathering plastics: An exploratory screening study with *Nitocra spinipes*," *Chemosphere*, vol. 132, pp. 114–119, Aug. 2015, doi: 10.1016/j.chemosphere.2015.03.010.
6. L. Bradney *et al.*, "Particulate plastics as a vector for toxic trace-element uptake by aquatic and terrestrial organisms and human health risk," *Environ. Int.*, vol. 131, p. 104937, Oct. 2019, doi: 10.1016/j.envint.2019.104937.
7. F. M. Lamberti, L. A. Román-Ramírez, and J. Wood, "Recycling of Bioplastics: Routes and Benefits," *J. Polym. Environ.*, vol. 28, no. 10, pp. 2551–2571, Oct. 2020, doi: 10.1007/s10924-020-01795-8.
8. OECD Global Plastics Outlook Database, "Plastic pollution is growing relentlessly as waste management and recycling fall short, says OECD," OECD. Accessed: May 08, 2023. [Online]. Available: https://www.oecd.org/environment/plastic-pollution-is-growing-relentlessly-as-waste-management-and-recycling-fall-short.htm
9. S. C. Dertinger *et al.*, "Technical pathways for distributed recycling of polymer composites for distributed manufacturing: Windshield wiper blades," *Resour. Conserv. Recycl.*, vol. 157, p. 104810, Jun. 2020, doi: 10.1016/j.resconrec.2020.104810.
10. S. Zhong and J. M. Pearce, "Tightening the loop on the circular economy: Coupled distributed recycling and manufacturing with recyclebot and RepRap 3-D printing," *Resour. Conserv. Recycl.*, vol. 128, pp. 48–58, Jan. 2018, doi: 10.1016/j.resconrec.2017.09.023.

11. F. A. Cruz Sanchez, H. Boudaoud, M. Camargo, and J. M. Pearce, "Plastic recycling in additive manufacturing: A systematic literature review and opportunities for the circular economy," *J. Clean. Prod.*, vol. 264, p. 121602, Aug. 2020, doi: 10.1016/j.jclepro.2020.121602.
12. H. A. Little, N. G. Tanikella, M. J. Reich, M. J. Fiedler, S. L. Snabes, and J. M. Pearce, "Towards Distributed Recycling with Additive Manufacturing of PET Flake Feedstocks," *Materials*, vol. 13, no. 19, p. 4273, Sep. 2020, doi: 10.3390/ma13194273.
13. M. A. Kreiger, M. L. Mulder, A. G. Glover, and J. M. Pearce, "Life cycle analysis of distributed recycling of post-consumer high density polyethylene for 3-D printing filament," *J. Clean. Prod.*, vol. 70, pp. 90–96, May 2014, doi: 10.1016/j.jclepro.2014.02.009.
14. M. Kreiger and J. M. Pearce, "Environmental Life Cycle Analysis of Distributed Three-Dimensional Printing and Conventional Manufacturing of Polymer Products," *ACS Sustain. Chem. Eng.*, vol. 1, no. 12, pp. 1511–1519, Dec. 2013, doi: 10.1021/sc400093k.
15. J. Gwamuri, B. T. Wittbrodt, N. C. Anzalone, and J. M. Pearce, "Reversing the Trend of Large Scale and Centralization in Manufacturing: The Case of Distributed Manufacturing of Customizable 3-D-Printable Self-Adjustable Glasses," *Chall. Sustain.*, vol. 2, no. 1, pp. 30–40, Dec. 2014, doi: 10.12924/cis2014.02010030.
16. E. Petersen and J. Pearce, "Emergence of Home Manufacturing in the Developed World: Return on Investment for Open-Source 3-D Printers," *Technologies*, vol. 5, no. 1, p. 7, Feb. 2017, doi: 10.3390/technologies5010007.
17. M. Mohammed, D. Wilson, E. Gomez-Kervin, A. Petsiuk, R. Dick, and J. M. Pearce, "Sustainability and feasibility assessment of distributed E-waste recycling using additive manufacturing in a Bi-continental context," *Addit. Manuf.*, vol. 50, p. 102548, Feb. 2022, doi: 10.1016/j.addma.2021.102548.
18. S. Zhong, P. Rakhe, and J. Pearce, "Energy Payback Time of a Solar Photovoltaic Powered Waste Plastic Recyclebot System," *Recycling*, vol. 2, no. 2, p. 10, Jun. 2017, doi: 10.3390/recycling2020010.
19. P. Santander, F. A. Cruz Sanchez, H. Boudaoud, and M. Camargo, "Social, political, and technological dimensions of the sustainability evaluation of a recycling network. A literature review," *Clean. Eng. Technol.*, vol. 6, p. 100397, Feb. 2022, doi: 10.1016/j.clet.2022.100397.
20. P. Santander, F. A. Cruz Sanchez, H. Boudaoud, and M. Camargo, "Closed loop supply chain network for local and distributed plastic recycling for 3D printing: a MILP-based optimization approach," *Resour. Conserv. Recycl.*, vol. 154, p. 104531, Mar. 2020, doi: 10.1016/j.resconrec.2019.104531.
21. C. Caceres Mendoza, P. Santander, F. Cruz-Sanchez, N. Troussier, M. Camargo, and H. Boudaoud, "Life Cycle Assessment of Distributed Plastic Recycling Via Additive Manufacturing," Sep. 26, 2022, *Rochester, NY*: 4230044. doi: 10.2139/ssrn.4230044.
22. A. O. Laplume, B. Petersen, and J. M. Pearce, "Global value chains from a 3D printing perspective," *J. Int. Bus. Stud.*, vol. 47, no. 5, pp. 595–609, Jun. 2016, doi: 10.1057/jibs.2015.47.
23. C. Baechler, M. DeVuono, and J. M. Pearce, "Distributed recycling of waste polymer into RepRap feedstock," *Rapid Prototyp. J.*, vol. 19, no. 2, pp. 118–125, Mar. 2013, doi: 10.1108/13552541311302978.
24. A. L. Woern, J. R. McCaslin, A. M. Pringle, and J. M. Pearce, "RepRapable Recyclebot: Open source 3-D printable extruder for converting plastic to 3-D printing filament," *HardwareX*, vol. 4, p. e00026, Oct. 2018, doi: 10.1016/j.ohx.2018.e00026.
25. R. Jones *et al.*, "RepRap – the replicating rapid prototyper," *Robotica*, vol. 29, no. 1, pp. 177–191, Jan. 2011, doi: 10.1017/S026357471000069X.
26. E. Sells, S. Bailard, Z. Smith, A. Bowyer, and V. Olliver, "RepRap: The Replicating Rapid Prototyper: Maximizing Customizability by Breeding the Means of Production," in *Handbook of Research in Mass Customization and Personalization*, World Scientific Publishing Company, 2009, pp. 568–580. doi: 10.1142/9789814280280_0028.
27. A. Bowyer, "3D Printing and Humanity's First Imperfect Replicator," *3D Print. Addit. Manuf.*, vol. 1, no. 1, pp. 4–5, Mar. 2014, doi: 10.1089/3dp.2013.0003.
28. F. Cruz Sanchez, S. Lanza, H. Boudaoud, S. Hoppe, and M. Camargo, "Polymer Recycling and Additive Manufacturing in an Open Source context : Optimization of processes and methods," Aug. 2015.
29. I. Anderson, "Mechanical Properties of Specimens 3D Printed with Virgin and Recycled Polylactic Acid," *3D Print. Addit. Manuf.*, vol. 4, no. 2, pp. 110–115, Jun. 2017, doi: 10.1089/3dp.2016.0054.
30. J. Pakkanen, D. Manfredi, P. Minetola, and L. Iuliano, "About the Use of Recycled or Biodegradable Filaments for Sustainability of 3D Printing," Apr. 2017, pp. 776–785. doi: 10.1007/978-3-319-57078-5_73.

31. M. I. Mohammed, D. Wilson, E. Gomez-Kervin, C. Vidler, L. Rosson, and J. Long, "The Recycling of E-Waste ABS Plastics by Melt Extrusion and 3D Printing Using Solar Powered Devices as a Transformative Tool for Humanitarian Aid," 2018, Accessed: Mar. 11, 2024. [Online]. Available: https://hdl.handle.net/2152/90080
32. S. Chong, G.-T. Pan, M. Khalid, T. C.-K. Yang, S.-T. Hung, and C.-M. Huang, "Physical Characterization and Pre-assessment of Recycled High-Density Polyethylene as 3D Printing Material," *J. Polym. Environ.*, vol. 2, no. 25, pp. 136–145, Jul. 2016, doi: 10.1007/s10924-016-0793-4.
33. M. Pepi, N. Zander, and M. Gillan, "Towards Expeditionary Battlefield Manufacturing Using Recycled, Reclaimed, and Scrap Materials," *JOM*, vol. 70, Jul. 2018, doi: 10.1007/s11837-018-3040-8.
34. N. Zander, M. Gillan, and R. Lambeth, "Recycled polyethylene terephthalate as a new FFF feedstock material," *Addit. Manuf.*, vol. 21, pp. 174–182, May 2018, doi: 10.1016/j.addma.2018.03.007.
35. N. Zander, "Recycled Polymer Feedstocks for Material Extrusion Additive Manufacturing," 2019, pp. 37–51. doi: 10.1021/bk-2019-1315.ch003.
36. K. R. Hart, J. B. Frketic, and J. R. Brown, "Recycling meal-ready-to-eat (MRE) pouches into polymer filament for material extrusion additive manufacturing," *Addit. Manuf.*, vol. 21, pp. 536–543, May 2018, doi: 10.1016/j.addma.2018.04.011.
37. S. Oberloier, N. G. Whisman, and J. M. Pearce, "Finding Ideal Parameters for Recycled Material Fused Particle Fabrication-Based 3D Printing Using an Open Source Software Implementation of Particle Swarm Optimization," *3D Print. Addit. Manuf.*, vol. 10, no. 6, pp. 1287–1300, Dec. 2023, doi: 10.1089/3dp.2022.0012.
38. A. L. Woern and J. M. Pearce, "Distributed Manufacturing of Flexible Products: Technical Feasibility and Economic Viability," *Technologies*, vol. 5, no. 4, Art. no. 4, Dec. 2017, doi: 10.3390/technologies5040071.
39. X. Tian, T. Liu, Q. Wang, A. Dilmurat, D. Li, and G. Ziegmann, "Recycling and remanufacturing of 3D printed continuous carbon fiber reinforced PLA composites," *J. Clean. Prod.*, vol. 142, pp. 1609–1618, Jan. 2017, doi: 10.1016/j.jclepro.2016.11.139.
40. A. Pringle, M. Rudnicki, and J. Pearce, "Wood Furniture Waste-Based Recycled 3-D Printing Filament," *For. Prod. J.*, vol. 68, Nov. 2017, doi: 10.13073/FPJ-D-17-00042.
41. P. Parandoush and D. Lin, "A review on additive manufacturing of polymer-fiber composites," *Compos. Struct.*, vol. 182, pp. 36–53, Dec. 2017, doi: 10.1016/j.compstruct.2017.08.088.
42. B. P. Heller, D. E. Smith, and D. A. Jack, "Planar deposition flow modeling of fiber filled composites in large area additive manufacturing," *Addit. Manuf.*, vol. 25, pp. 227–238, Jan. 2019, doi: 10.1016/j.addma.2018.10.031.
43. A. Romani, L. Perusin, M. Ciurnelli, and M. Levi, "Characterization of PLA feedstock after multiple recycling processes for large-format material extrusion additive manufacturing," *Mater. Today Sustain.*, vol. 25, p. 100636, Mar. 2024, doi: 10.1016/j.mtsust.2023.100636.
44. J. M. Justino Netto, H. T. Idogava, L. E. Frezzatto Santos, Z. de C. Silveira, P. Romio, and J. L. Alves, "Screw-assisted 3D printing with granulated materials: a systematic review," *Int. J. Adv. Manuf. Technol.*, vol. 115, no. 9, pp. 2711–2727, Aug. 2021, doi: 10.1007/s00170-021-07365-z.
45. M. J. Reich, A. L. Woern, N. G. Tanikella, and J. M. Pearce, "Mechanical Properties and Applications of Recycled Polycarbonate Particle Material Extrusion-Based Additive Manufacturing," *Materials*, vol. 12, no. 10, Art. no. 10, Jan. 2019, doi: 10.3390/ma12101642.
46. A. Romani, M. Levi, and J. M. Pearce, "Recycled polycarbonate and polycarbonate/acrylonitrile butadiene styrene feedstocks for circular economy product applications with fused granular fabrication-based additive manufacturing," *Sustain. Mater. Technol.*, vol. 38, p. e00730, Dec. 2023, doi: 10.1016/j.susmat.2023.e00730.
47. C. Suescun Gonzalez, F. A. Cruz Sanchez, H. Boudaoud, C. Nouvel, and J. M. Pearce, "Multi-material distributed recycling via material extrusion: recycled high density polyethylene and poly (ethylene terephthalate) mixture," *Polym. Eng. Sci.*, vol. 64, no. 4, pp. 1555–1570, 2024, doi: 10.1002/pen.26643.
48. A. Alexandre, F. A. Cruz Sanchez, H. Boudaoud, M. Camargo, and J. M. Pearce, "Mechanical Properties of Direct Waste Printing of Polylactic Acid with Universal Pellets Extruder: Comparison to Fused Filament Fabrication on Open-Source Desktop Three-Dimensional Printers," *3D Print. Addit. Manuf.*, vol. 7, no. 5, pp. 237–247, Oct. 2020, doi: 10.1089/3dp.2019.0195.
49. A. Woern, D. Byard, R. Oakley, M. Fiedler, S. Snabes, and J. Pearce, "Fused Particle Fabrication 3-D Printing: Recycled Materials' Optimization and Mechanical Properties," *Materials*, vol. 11, no. 8, p. 1413, Aug. 2018, doi: 10.3390/ma11081413.
50. S. Whyman, K. M. Arif, and J. Potgieter, "Design and development of an extrusion system for 3D printing biopolymer pellets," *Int. J. Adv. Manuf. Technol.*, vol. 96, no. 9, pp. 3417–3428, Jun. 2018, doi: 10.1007/s00170-018-1843-y.

51. M. Paramatti, A. Romani, G. Pugliese, and M. Levi, "PLA Feedstock Filled with Spent Coffee Grounds for New Product Applications with Large-Format Material Extrusion Additive Manufacturing," *ACS Omega*, vol. 9, no. 6, pp. 6423–6431, Feb. 2024, doi: 10.1021/acsomega.3c05669.
52. N. Volpato, D. Kretschek, J. A. Foggiatto, and C. M. Gomez da Silva Cruz, "Experimental analysis of an extrusion system for additive manufacturing based on polymer pellets," *Int. J. Adv. Manuf. Technol.*, vol. 81, no. 9, pp. 1519–1531, Dec. 2015, doi: 10.1007/s00170-015-7300-2.
53. D. Byard, A. Woern, R. Oakley, M. Fiedler, S. Snabes, and J. Pearce, "Green fab lab applications of large-area waste polymer-based additive manufacturing," *Addit. Manuf.*, vol. 27, pp. 515–525, May 2019, doi: 10.1016/j.addma.2019.03.006.
54. W. d'Ambrières, "Plastics recycling worldwide: current overview and desirable changes," *Field Actions Sci. Rep. J. Field Actions*, no. Special Issue 19, Art. no. Special Issue 19, Mar. 2019.
55. B. Ruj, V. Pandey, P. Jash, and V. Srivastava, "Sorting of plastic waste for effective recycling," *Int J Appl Sci Eng Res*, vol. 4, Jan. 2015, doi: 10.6088/ijaser.04058.
56. S. Wang, L. Capoen, D. R. D'hooge, and L. Cardon, "Can the melt flow index be used to predict the success of fused deposition modelling of commercial poly(lactic acid) filaments into 3D printed materials?," *Plast. Rubber Compos.*, Feb. 2018, Accessed: Jul. 16, 2024. [Online]. Available: https://journals.sagepub.com/doi/full/10.1080/14658011.2017.1397308
57. M. Spoerk, J. Gonzalez-Gutierrez, J. Sapkota, S. Schuschnigg, and C. Holzer, "Effect of the printing bed temperature on the adhesion of parts produced by fused filament fabrication," *Plast. Rubber Compos.*, vol. 47, no. 1, pp. 17–24, Feb. 2018, doi: 10.1080/14658011.2017.1399531.
58. S. Guerreiro, I. João, and L. Pimentel Real, "Evaluation of the influence of testing parameters on the melt flow index of thermoplastics," *Polym. Test.*, vol. 31, pp. 1026–1030, Dec. 2012, doi: 10.1016/j.polymertesting.2012.07.008.
59. M. Teresa Rodríguez-Hernández, J. L. Angulo-Sánchez, and A. Pérez-Chantaco, "Determination of the molecular characteristics of commercial polyethylenes with different architectures and the relation with the melt flow index," *J. Appl. Polym. Sci.*, vol. 104, no. 3, pp. 1572–1578, 2007, doi: 10.1002/app.25625.
60. A. V. Shenoy and D. R. Saini, "Melt flow index: More than just a quality control rheological parameter. Part I," *Adv. Polym. Technol.*, vol. 6, no. 1, pp. 1–58, 1986, doi: 10.1002/adv.1986.060060101.
61. R. V. Pazhamannil, J. N. V. N., G. P., and A. Edacherian, "Property enhancement approaches of fused filament fabrication technology: A review," *Polym. Eng. Sci.*, vol. 62, no. 5, pp. 1356–1376, 2022, doi: 10.1002/pen.25948.
62. E. E. Ferg and L. L. Bolo, "A correlation between the variable melt flow index and the molecular mass distribution of virgin and recycled polypropylene used in the manufacturing of battery cases," *Polym. Test.*, vol. 32, no. 8, pp. 1452–1459, Dec. 2013, doi: 10.1016/j.polymertesting.2013.09.009.
63. B. Singh *et al.*, "Investigations on Melt Flow Rate and Tensile Behaviour of Single, Double and Triple-Sized Copper Reinforced Thermoplastic Composites," *Materials*, vol. 14, no. 13, Art. no. 13, Jan. 2021, doi: 10.3390/ma14133504.
64. R. Plavec *et al.*, "Influence of Multiple Thermomechanical Processing of 3D Filaments Based on Polylactic Acid and Polyhydroxybutyrate on Their Rheological and Utility Properties," *Polymers*, vol. 14, no. 10, Art. no. 10, Jan. 2022, doi: 10.3390/polym14101947.
65. N. Sa'ude, K. Kamarudin, M. Ibrahim, and M. H. I. Ibrahim, "Melt Flow Index of Recycle ABS for Fused Deposition Modeling (FDM) Filament," *Appl. Mech. Mater.*, vol. 773–774, pp. 3–7, 2015, doi: 10.4028/www.scientific.net/AMM.773-774.3.
66. F. Laoutid, S. Lafqir, A. Toncheva, and P. Dubois, "Valorization of Recycled Tire Rubber for 3D Printing of ABS- and TPO-Based Composites," *Materials*, vol. 14, no. 19, Art. no. 19, Jan. 2021, doi: 10.3390/ma14195889.
67. M. Garwacki, I. Cudnik, D. Dziadowiec, P. Szymczak, and J. Andrzejewski, "The Development of Sustainable Polyethylene Terephthalate Glycol-Based (PETG) Blends for Additive Manufacturing Processing—The Use of Multilayered Foil Waste as the Blend Component," *Materials*, vol. 17, no. 5, Art. no. 5, Jan. 2024, doi: 10.3390/ma17051083.
68. A. Gupta, M. Misra, and A. K. Mohanty, "Novel sustainable materials from waste plastics: compatibilized blend from discarded bale wrap and plastic bottles," *RSC Adv.*, vol. 11, no. 15, pp. 8594–8605, Feb. 2021, doi: 10.1039/D1RA00254F.
69. V. Kumar, R. Singh, and I. P. S. Ahuja, "On correlation of rheological, thermal, mechanical and morphological properties of chemical assisted mechanically blended ABS-Graphene composite as tertiary recycling for 3D

printing applications," *Adv. Mater. Process. Technol.*, Jul. 2022, Accessed: Jul. 22, 2024. [Online]. Available: https://www.tandfonline.com/doi/abs/10.1080/2374068X.2021.1913324

70. E. O. Cisneros-López *et al.*, "Recycled poly(lactic acid)–based 3D printed sustainable biocomposites: a comparative study with injection molding," *Mater. Today Sustain.*, vol. 7–8, p. 100027, Mar. 2020, doi: 10.1016/j.mtsust.2019.100027.
71. O. Zabihi *et al.*, "Mechanical upcycling of single-use face mask waste into high-performance composites: An ecofriendly approach with cost-benefit analysis," *Sci. Total Environ.*, vol. 919, p. 170469, Apr. 2024, doi: 10.1016/j.scitotenv.2024.170469.
72. V. Mishra, C. K. Ror, S. Negi, S. Kar, and L. N. Borah, "Development of sustainable 3D printing filaments using recycled/virgin ABS blends: Processing and characterization," *Polym. Eng. Sci.*, vol. 63, no. 7, pp. 1890–1899, 2023, doi: 10.1002/pen.26330.
73. I. Turku, S. Kasala, and T. Kärki, "Characterization of Polystyrene Wastes as Potential Extruded Feedstock Filament for 3D Printing," *Recycling*, vol. 3, no. 4, Art. no. 4, Dec. 2018, doi: 10.3390/recycling3040057.
74. "MXBAOHENG XNR-400B Melt Flow Rate Index Tester MFR Melt Flow Indexer Printing Machine (220V) : Amazon.ca: Tools & Home Improvement." Accessed: Jul. 17, 2024. [Online]. Available: https://www.amazon.ca/MXBAOHENG-XNR-400B-Indexer-Printing-Machine/dp/B07CMN9SWN?th=1
75. "Wholesale melt flow index mfi testing machine To Test Electronic Equipment - Alibaba.com." Accessed: Mar. 15, 2024. [Online]. Available: https://www.alibaba.com/showroom/melt-flow-index-mfi-testing-machine.html
76. "MELT FLOW INDEXER-tabletop instrument that tests the melt mass." Accessed: Mar. 15, 2024. [Online]. Available: https://www.mrclab.com/melt-flow-indexer-1
77. D. Liu and A. Romani, "MFI," Jun. 2023, Accessed: Jul. 24, 2024. [Online]. Available: https://osf.io/68hbj/
78. "Teensy® 4.0." Accessed: Mar. 11, 2024. [Online]. Available: https://www.pjrc.com/store/teensy40.html
79. V. Klar, J. M. Pearce, P. Kärki, and P. Kuosmanen, "Ystruder: Open source multifunction extruder with sensing and monitoring capabilities," *HardwareX*, vol. 6, p. e00080, Oct. 2019, doi: 10.1016/j.ohx.2019.e00080.
80. 14:00-17:00, "ISO 1133-1:2022," ISO. Accessed: Jul. 16, 2024. [Online]. Available: https://www.iso.org/standard/83905.html
81. "compass." Accessed: Jul. 16, 2024. [Online]. Available: https://compass.astm.org/document/?contentCode=ASTM%7CD1238-10%7Cen-US&proxycl=https%3A%2F%2Fsecure.astm.org&fromLogin=true
82. M. Y. T. Wu, S. L. Mak, W. F. Tang, C. H. Li, and T. W. Chan, "A Review on Melt Flow Index Characteristics of Polylactide (PLA) for Recycle Use in 3-D Printing," *J. Test. Eval.*, vol. 50, no. 4, pp. 2260–2267, 2022, doi: 10.1520/JTE20210314.
83. M. H. M. Nasir, M. M. Taha, N. Razali, R. A. Ilyas, V. F. Knight, and M. N. F. Norrrahim, "Effect of Chemical Treatment of Sugar Palm Fibre on Rheological and Thermal Properties of the PLA Composites Filament for FDM 3D Printing," *Materials*, vol. 15, no. 22, Art. no. 22, Jan. 2022, doi: 10.3390/ma15228082.
84. F. Doronin, A. Rudakova, G. Rytikov, and V. Nazarov, "A novel determination of the melt flow index of composite filaments used in extrusion additive manufacturing," *Polym. Test.*, vol. 133, p. 108376, Apr. 2024, doi: 10.1016/j.polymertesting.2024.108376.
85. V. K n, D. Bonthu, M. Doddamani, and F. Pati, "Additive Manufacturing of Short Silk Fiber Reinforced PETG Composites," *Mater. Today Commun.*, vol. 33, p. 104772, Dec. 2022, doi: 10.1016/j.mtcomm.2022.104772.
86. S. V. Kotomin, D. V. Kramarev, I. M. Obidin, and S. V. Polunin, "Influence of 3D Printing Conditions of Polyethylene Terephthalate Glycol on the Mechanical Properties of Products Based on It," *Polym. Sci. Ser. A*, vol. 64, no. 6, pp. 617–623, Dec. 2022, doi: 10.1134/S0965545X22700365.
87. R. Singh *et al.*, "On 3D printing of low-cost sensors using recycled PET," *Sādhanā*, vol. 47, no. 4, p. 260, Nov. 2022, doi: 10.1007/s12046-022-02029-4.
88. "PolyLite_PETG_TDS_V5.2.pdf." Accessed: Jul. 24, 2024. [Online]. Available: https://cdn.shopify.com/s/files/1/0548/7299/7945/files/PolyLite_PETG_TDS_V5.2.pdf?v=1640828798
89. M. Bustos Seibert, G. A. Mazzei Capote, M. Gruber, W. Volk, and T. A. Osswald, "Manufacturing of a PET Filament from Recycled Material for Material Extrusion (MEX)," *Recycling*, vol. 7, no. 5, Art. no. 5, Oct. 2022, doi: 10.3390/recycling7050069.
90. M. Nofar and H. Oğuz, "Development of PBT/Recycled-PET Blends and the Influence of Using Chain Extender," *J. Polym. Environ.*, vol. 27, no. 7, pp. 1404–1417, Jul. 2019, doi: 10.1007/s10924-019-01435-w.
91. "Ingeo Biopolymer 4043D Technical Data Sheet".

92. M. Seifali Abbas-Abadi, M. Nekoomanesh Haghighi, H. Yeganeh, and B. Bozorgi, "The effect of melt flow index, melt flow rate, and particle size on the thermal degradation of commercial high density polyethylene powder," *J. Therm. Anal. Calorim.*, vol. 114, no. 3, pp. 1333–1339, Dec. 2013, doi: 10.1007/s10973-013-3133-0.
93. S. S. Bafna and A.-M. Beall, "A Design of Experiments Study on the Factors Affecting Variability in the Melt Index Measurement".
94. A. Shenoy and D. Saini, "Melt flow index: More than just a quality control rheological parameter. Part II," *Adv. Polym. Technol. - ADV POLYM TECHNOL*, vol. 6, pp. 125–145, Jun. 1986, doi: 10.1002/adv.1986.060060201.
95. S. K. Suman and V. K. Giri, "Speed control of DC motor using optimization techniques based PID Controller," in *2016 IEEE International Conference on Engineering and Technology (ICETECH)*, Coimbatore, India: IEEE, Mar. 2016, pp. 581–587. doi: 10.1109/ICETECH.2016.7569318.